CALIFORNIA ENERGY COMMISSION

CALIFORNIA NATURAL RESOURCES AGENCY

ENERGY RESEARCH AND DEVELOPMENT DIVISION

FINAL PROJECT REPORT

High Efficiency Process Heating

March 2024 | CEC-500-2024-004

PREPARED BY:

David Cygan
Hamid Abbasi
GTI Energy
1700 S. Mount Prospect Rd.
Des Plaines, IL 60563
(847) 768-0524
www.gti.energy
Primary Authors

Michael Lozano
Commission Agreement Manager

Agreement Number: PIR-17-017

Virginia Lew
Office Manager
ENERGY EFFICIENCY RESEARCH OFFICE

Jonah Steinbuck, Ph.D.
Director
ENERGY RESEARCH AND DEVELOPMENT DIVISION

Drew Bohan
Executive Director

ACKNOWLEDGEMENTS

This project was co-sponsored by the California Energy Commission (CEC) and the Advanced Research Project Agency – Energy (ARPA-E) of the U.S. Department of Energy (DOE). GTI Energy (GTI) gratefully acknowledges the assistance of CEC and DOE/ARPA-E representatives for their project guidance, support, and input on technical matters. In addition, cost-sharing for this project was provided by the Southern California Gas Company, Utilization Technology Development NFP and University of California at Merced (UCM). Sub-contractors for the project were UCM, Particulate Solid Research Inc. and Stanley Consultants (Stanley). Recognition of individuals from these organizations who made key contributions to the project is provided below.

- CEC: Michael Lozano
- DOE/ARPA-E: Dr. Peter de Bock, Dr. Rachel Slaybaugh, Dr. Eric Schiff, Dr. Howard Branz, Dr. James Zahler, and Dr. Brian Borak (Contractor)
- UCM: Professor Roland Winston, Dr. Lun Jiang, Dr. Bennett Widyolar, Dr. Yogesh Bhusal, and Jonathan Ferry - collector/receiver/absorber design and testing; Professor James Palko, Souvik Roy and Gokce Ozkazanc-Guc - receiver modeling
- PSRI: Dr. Reddy Karri and John Findlay - particle transport and storage system
- GTI: Joseph Pondo - particle transport and storage system installation, controls, and testing
- Stanley: Lance Rowell, Chris DePodesta, and Jeremy Owen - conceptual and preliminary engineering and technology transfer.

PREFACE

The California Energy Commission's (CEC) Energy Research and Development Division manages the Natural Gas Research and Development Program, which supports energy-related research, development, and demonstration not adequately provided by competitive and regulated markets. These natural gas research investments spur innovation in energy efficiency, renewable energy and advanced clean generation, energy-related environmental protection, energy transmission and distribution and transportation.

The Energy Research and Development Division conducts this public interest natural gas-related energy research by partnering with RD&D entities, including individuals, businesses, utilities and public and private research institutions. This program promotes greater natural gas reliability, lower costs and increases safety for Californians and is focused in these areas:

- Buildings End-Use Energy Efficiency.
- Industrial, Agriculture and Water Efficiency
- Renewable Energy and Advanced Generation
- Natural Gas Infrastructure Safety and Integrity.
- Energy-Related Environmental Research
- Natural Gas-Related Transportation.

This is the final report for the High Efficiency Process Heating project (Grant Number PIR-17-017) conducted by GTI Energy and University of California, Merced. The information from this project contributes to the Energy Research and Development Division's Natural Gas Research and Development Program.

For more information about the Energy Research and Development Division, please visit the CEC's research website (www.energy.ca.gov/research/) or contact the Energy Research and Development Division at ERDD@energy.ca.gov.

ABSTRACT

GTI Energy collaborated with the University of California at Merced to upscale the solar thermal transport and storage technology. The solar thermal transport and storage technology integrates a two-stage concentrating solar collector with a particle thermal transport and storage system to provide cost-effective, on-demand high temperature industrial process heat of up to 1,112 degrees Fahrenheit (ºF) (600 degrees Celsius (ºC). The aim was to demonstrate the technology at an industrial site to reduce process heating fuel usage and the carbon footprint. The team developed a conceptual system design for the host site retrofit, including heat balance, process flow diagram, and equipment placements. University of California at Merced designed and tested the two-stage collector with multiple connected four-meter-long receivers, while GTI focused on a matching 1,202 °F (650 °C) capable particle thermal transport and storage system. On-sun testing at University of California at Merced revealed bending issues with the absorber tubes under the intense solar radiation generated on the absorber in the two-stage collector. To address the bending issue, a self-consistent iterative model, comprising integrated illumination, thermal, and deformation modules was developed. The model was used to optimize the absorber tube length, considering deformation, overall collector efficiency, and installation complexity, resulting in a 2.7-meter recommended absorber length. The associated particle thermal transport and storage system was successfully designed, built and tested, demonstrating stable particle flow rate, minimal particle degradation and acceptable pressure drop. Collaborating with Stanley Consultants, the team prepared conceptual and preliminary engineering packages to support future development and commercialization efforts. They included diagrams, project definitions, cost estimates, and market evaluation for a 2-megawatt thermal system. The time and efforts spent in addressing the absorber bending issues, however, prevented the team from moving ahead with field demonstration of the system within available project budget and schedule.

Keywords: High intensity parabolic collector, two stage receiver, refractory particles, particle thermal fluid, particle thermal storage, solar process heating, high temperature solar thermal, dense phase particle transport and 2-megawatt thermal solar system.

Please use the following citation for this report:

Cygan, David, and Hamid Abbasi. 2023. *High Efficiency Process Heating*. California Energy Commission. Publication Number: CEC-500-2024-004.

TABLE OF CONTENTS

LIST OF FIGURES

LIST OF TABLES

Executive Summary

Background

Gas Technology Institute and University of California, Merced conceived and developed solar thermal transport and storage technology that could significantly reduce natural gas use in industrial process heating. The technology uses two-stage high intensity parabolic collectors to capture and store energy in inert refractory particles for on-demand use. Solar thermal transport and storage enables high temperature process heat up to 1,112 degrees Fahrenheit (°F), (600 degrees Celsius [°C]), expanding solar thermal application in industry. The use of inert refractory particles to capture, store, and transport energy eliminates safety and cost issues associated with other high temperature energy storage technologies. On-sun testing at a 5-kilowatt scale in a previous Advanced Research Project Agency – Energy of the U.S. Department of Energy-funded project demonstrated up to 1,265 °F (685 °C) particle heating capability, proving its value for industrial customers, with potential for broad market deployment and substantial natural gas savings in California.

Project Purpose

This project aimed to develop the solar thermal transport and storage technology to: 1) deliver supplemental solar thermal energy to the gypsum kettle at the USG Corporation facility that was the field test site; 2) confirm seamless integration into existing infrastructure of the plant; 3) ensure straightforward installation and reliable operation; and 4) achieve a greater than 20 percent reduction in natural gas use, and a payback period of less than five years. The project's goal was to demonstrate the technology in an industrial process heating application, independently verifying its performance, energy savings, and emissions benefits.

Project Approach

Gas Technology Institute and its partners were responsible for designing, building, and testing a 17-meter-long prototype collector at University of California, Merced, along with a matching particle thermal fluid loop with storage at Gas Technology Institute. The collector and the particle thermal fluid loop were designed and constructed for testing at University of California, Merced and Gas Technology Institute, respectively, and then be transported to the host site for installation, commissioning, and evaluation over an extended monitoring period to assess its performance relative to the project goals. Independent measurement and verification of system performance, energy savings, and emissions benefits would be conducted. The results would be widely disseminated to facilitate technology transfer to industrial users in California, promoting awareness and adoption of the solar thermal transport and storage process heating technology and reducing natural gas consumption. The proposed demonstration of the full-scale nominal 50-kilowatt collector at an industrial site was crucial for independently quantifying the performance, energy efficiency gains and greenhouse gas emission benefits. The installation knowledge and insights gained would provide valuable information for potential host sites and contractors. However, due to complications with the solar thermal transport and storage prototype, the field demonstration did not occur as described in the next section.

Project Results

The research team developed a conceptual system design for host site retrofit, including a preliminary heat balance, process flow diagram, and equipment placements. Efforts were made at University of California, Merced to design, build, and test a 17-meter-long commercial-scale prototype collector system, while Gas Technology Institute worked on designing, building, and testing a matching particle thermal transport and storage system. A four-meter-long receiver was fabricated and successfully tested at 1,202 °F (650 °C) in a laboratory setting. A 17-meter-long parabolic trough was installed at University of California, Merced for on-sun testing, and several 4-meter-long receivers were built. On-sun testing at University of California, Merced revealed bending issues with the absorber tubes under the intense solar radiation generated on the absorber in the two-stage collector. To address this, an algorithm that integrated illumination, thermal behavior and deformation analysis modules in a single iterative model was developed to determine the absorber length for optimum thermal and mechanical performance, while minimizing its bending. The model recommended a shorter absorber length of 2.7 meters as optimum to minimize bending and achieve high capture efficiency. In parallel, the particle thermal transport and storage system was successfully tested at Gas Technology Institute, demonstrating minimal particle degradation and low-pressure drop in the piping. However, the time and efforts spent in addressing the absorber bending issues, prevented the team from moving ahead with field demonstration of the system.

Though the field demonstration did not occur, the team collaborated with Stanley Consultants (Stanley) to prepare engineering packages for future development and commercialization. These included system diagrams, project definitions, cost estimates, and market evaluation for a 2-megawatt therm solar thermal transport and storage system.

Technology/Knowledge Transfer/Market Adoption (Advancing the Research to Market)

Gas Technology Institute collaborated with the University of Chicago Booth School of Business and Stanley Consultants to develop a commercialization plan for the solar thermal transport and storage technology. Feedback and insights were gathered from industry leaders representing various sectors. The plan covered products and services, market drivers, operations, research and development, distribution strategy, market analysis, marketing approach, competition, financial model, licensing options, and exit analysis. Customer targets are food manufacturing in sunny areas, as well as gas-fueled process heating furnaces, steel and metals manufacturing, thermal storage, and commercial HVAC systems. Discussions were held with selected potential partners and stakeholders.

The estimated timeline for the project, from preliminary engineering to a 2-megawatt therm solar thermal transport and storage plant, was estimated to be 24 months. However, it took longer due to bending issues with the absorber tubes. After the bending issues were resolved, it was determined that the manufacturing of the particle thermal transport and storage system can use standard engineering and manufacturing techniques, while the specialized solar receiver components require precision and quality control. For this reason, it is recommended

to source standard components from third parties and fabricate the receiver components in-house.

The marketing approach focused on acquiring, retaining, and growing customers through pilot programs. Several publications and presentations were made to disseminate the project's findings, including journal articles, papers, symposiums, and seminars hosted by University of California, Merced, Advanced Research Project Agency – Energy, and Southern California Gas Company.

Gas Technology Institute is currently demonstrating the particle thermal transport and storage technology component of the solar thermal transport and storage technology in a follow-on project funded by the US Department of Defense through Worcester Polytechnic Institute. The particle thermal transport and storage technology is suitable for heat recovery from exhaust gases of a wide range of industrial processes, both continuous and batch types, and has the potential for significant natural gas savings and carbon reductions in California.

Benefits to California

The successful deployment of solar thermal transport and storage technology has the potential to offer to reduce natural gas demand in California's industrial sector, benefiting rate payers and industrial facilities. The technology has the potential to enable sustainable energy use, lower natural gas costs, and reduce operational cost for industrial facilities. The widespread adoption of solar thermal transport and storage technology could provide environmental benefits and deliver substantial cost savings throughout the life cycle.

In California, approximately 200 trillion British thermal units per year of natural gas are used for industrial process heating, which accounts for about 30 percent of the total natural gas consumption in this sector. With an estimated 20 percent efficiency gain and 10 percent market penetration, the solar thermal transport and storage technology has the potential to achieve annual natural gas savings of over four trillion British thermal units, translating to $40 million in energy cost savings for industrial customers (assuming a gas price of $10 per million British thermal units). This adoption could lead to reductions in greenhouse gas and nitrogen oxide emissions, surpassing 212,000 metric tons of carbon dioxide equivalent emissions per year and 218 metric tons of nitrogen oxide annually.

In summary, the solar thermal transport and storage technology, with successful implementation and testing of recommended design improvements, has the potential to revolutionize the field of process heating by offering a renewable and sustainable alternative to conventional solutions. By implementing the above recommendations, the commercialization and widespread adoption of this technology can be possible, leading to a more environmentally friendly and efficient approach to meeting industrial heating needs.

CHAPTER 1: Introduction

Technology Background

Gas Technology Institute (GTI) and the University of California at Merced (UCM) conceived and developed solar thermal transport and storage (STTS) technology that can significantly reduce natural gas use in industrial process heating. The technology uses two-stage high intensity parabolic collectors to capture and store energy in inert refractory particles for on-demand use. STTS enables high temperature process heat up to 1,112 degrees Fahrenheit (°F) (600 degrees Celsius [°C]), expanding solar thermal application in industry. The use of inert refractory particles to capture, store and transport energy eliminates safety and cost issues associated with other high temperature energy storage technologies. On sun testing at a 5-kilowatt (kW) scale in a previous Advanced Research Project Agency – Energy (DOE ARPA-E) funded project demonstrated up to 1,265 °F (685 °C) particle heating capability, proving its value for industrial customers, with potential for broad market deployment and substantial natural gas savings in California.

Figure 1 shows the original concept of the STTS receiver. It consists of an outer glass tube surrounding the absorber and the secondary Alanod reflector. Radiation from the primary parabolic reflector that bypasses the absorber tube is captured by the secondary reflector and focused on the back of the absorber. This allows the absorber to be heated from all sides, improving temperature uniformity, and increasing heat transfer to the thermal fluid inside the absorber.

Figure 1: High temperature receiver with secondary

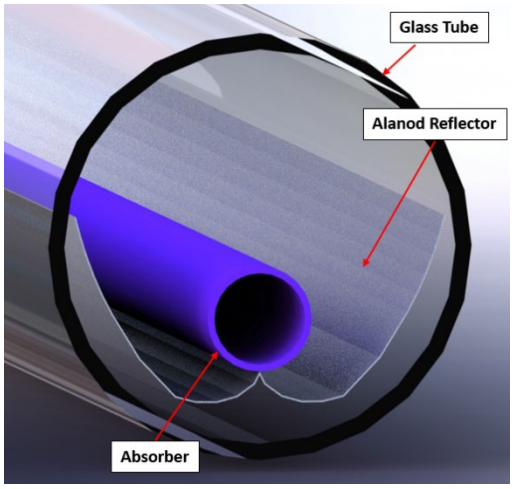

Figure 2 illustrates a version of the particle thermal transport and storage (TTS) process. During the daytime, excess thermal energy is directed from the receivers to the hot separator storage, where hot particles are separated and stored. The hot gases flow to the cold particle storage, where they heat the cold particles before being directed back to the receiver tube. During the night, the process is reversed to supply additional thermal energy for process

heating. The STTS technology enables storage and recovery of solar energy at temperatures up to 1,202 °F (650 °C) and potentially even higher, using particle-based thermal fluid systems that offer advantages over traditional molten salts.

Figure 2: Particle thermal transport and storage

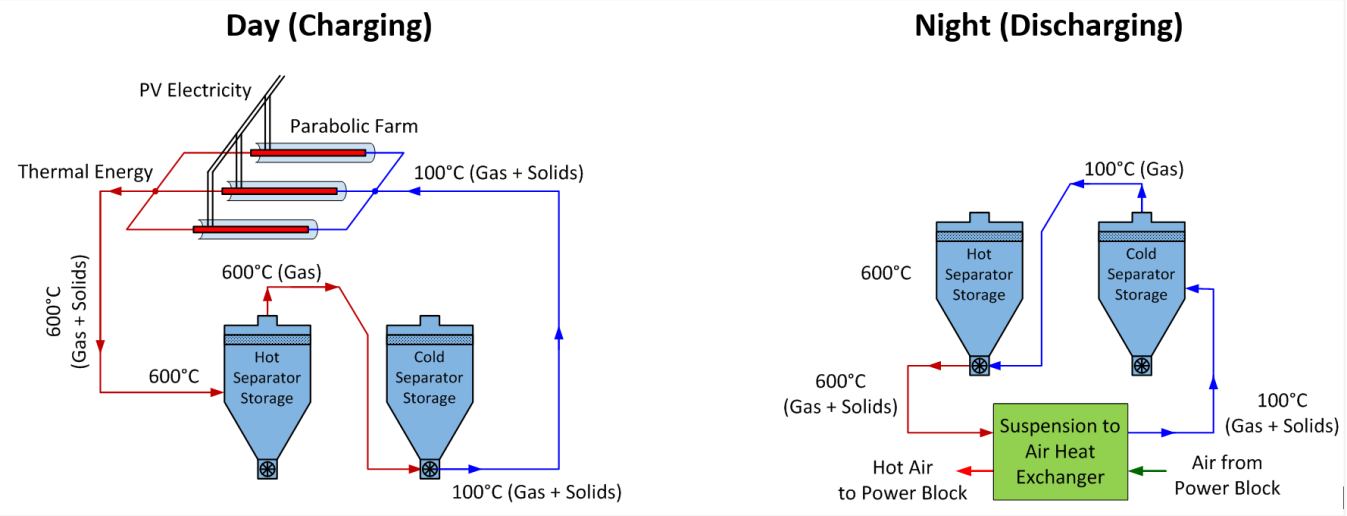

The STTS technology uses a modular and scalable parabolic trough collector design, making it suitable for replacing natural gas in various industrial processes. Parabolic collector fields are low-cost, have a proven track record of continuous operation, and tolerate larger optical errors compared to other technologies. The particle-based thermal capture, transport, storage, and recovery system in the STTS technology enables the use of a single flow loop, offers a wide range of particle material options, and eliminates the direct link between temperature and pressure of conventional thermal fluids. It also provides advantages over molten salts, such as relative temperature insensitivity of viscosity, avoidance of solidification/freezing concerns, absence of side reactions, non-corrosiveness, and potential for much higher temperatures.

The high temperature concentrating solar collector and the particle-based thermal fluid system—the two major components of the STTS technology—had undergone successful design, construction, and testing at UCM and GTI, respectively, at a nominal 5 kilowatts thermal (kWth) input scale using a one-meter-long collector. These components were subjected to multiple test campaigns and design upgrades over the past several years, supported by funding from ARPA-E and the US gas industry. The integration of the high-temperature receiver and particle thermal fluid system had been tested previously at UCM at the 5-kWth scale to convert solar energy into greater than 1,112 °F (600 °C) particle thermal fluid for on-demand use.

Figure 3 shows the fully assembled one-meter-long receiver designed for a nominal 5-kWth peak solar input. The metal absorber tube is covered with a low emissivity coating and enclosed within a borosilicate vacuum tube.

Figure 3: One-meter-long high temperature thermal receiver

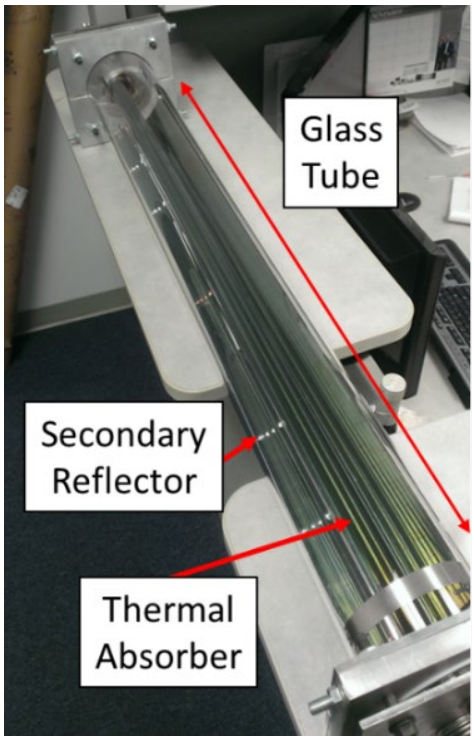

Source: UCM

On-sun optical efficiency tests using water as the thermal fluid demonstrated an average output of 2.45 kWth at a solar input of 3.5 kWth, achieving an optical efficiency of 70 percent, which is close to the design value of 72 percent (Figure 4).

Figure 4: Optical efficiency of test absorber

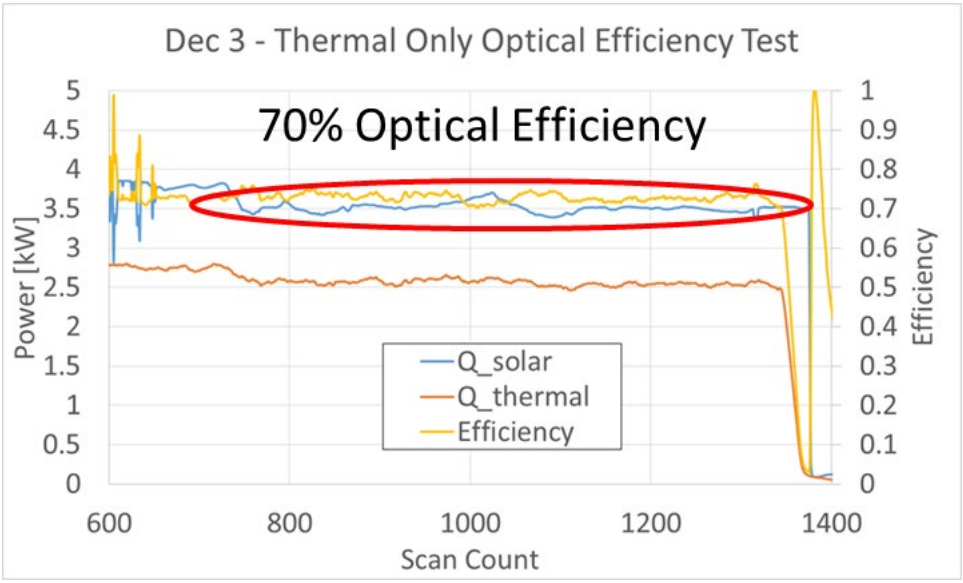

Figure 5 shows the particle thermal fluid test loop at GTI. It allows simulation of any one-meter-long (5 kWth) section of a full-scale receiver because it can deliver particles to the receiver at any temperature from ambient to about 1,112 °F (600 °C). Tests conducted at GTI

achieved particle thermal fluid temperatures of 1,076 °F (580 °C), with no adverse effects to particles or flow path observed over multiple charge-discharge cycles. The pumping power required was minimal, and the system pressures remained within acceptable ranges. The particle-air suspension exhibited high heat transfer rates, which would prevent overheating of the absorber.

Figure 5: Particle test loop with storage

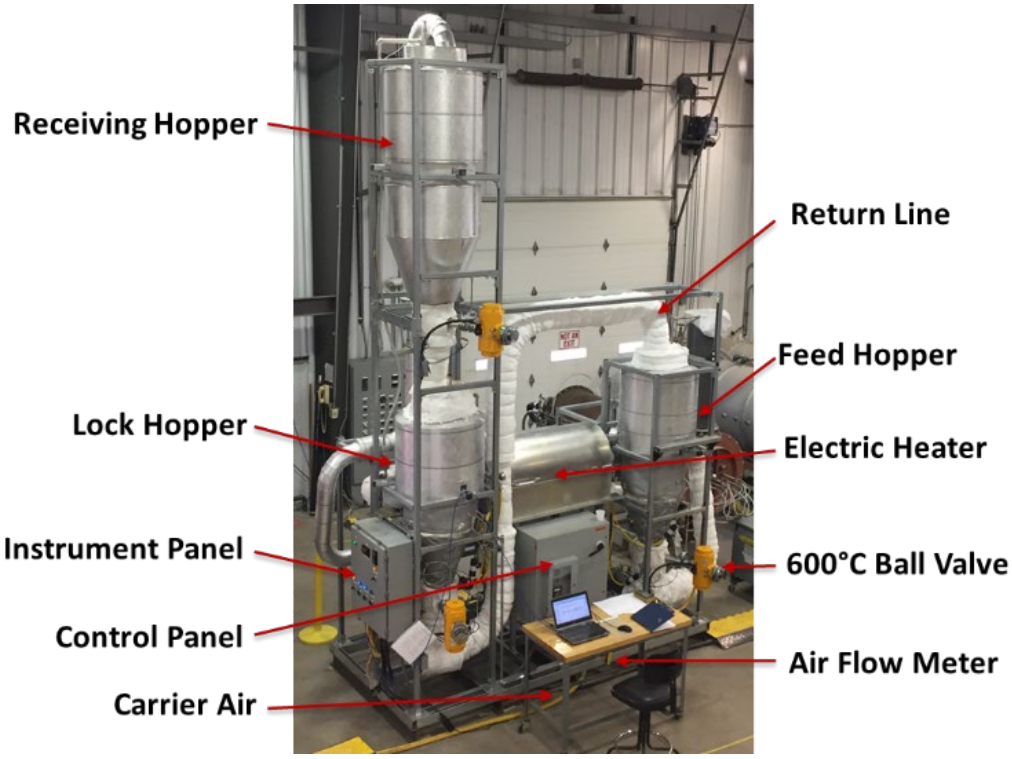

Source: GTI

Figure 6 shows the integrated one-meter-long, nominal 5 kWth STTS system at UCM, combining the collector and the particle test loop. The left photograph shows the overall system, and the right photograph shows the intensity of the absorber radiation during on-sun testing. Heat-up and cool-down tests were conducted on the integrated system to characterize its operation.

Figure 6: Nominal 5 kWth STTS test system (left) and intensity of absorber radiation during on-sun tests (right)

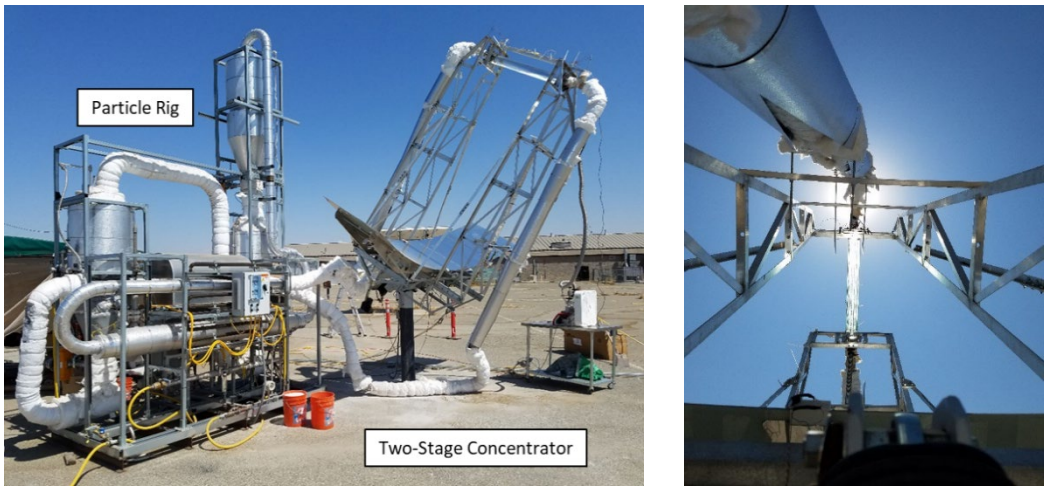

Source: UCM

Figure 7 plots the inlet and outlet temperatures of the receiver during these tests showing particle temperatures reaching 1,265 °F (685 °C), exceeding the target of 1,202 °F (650 °C). These tests also allowed acquisition of data for scale up to a full-scale collector with integrated particle transport and storage.

Figure 7: Absorber outlet temperature during integrated system testing

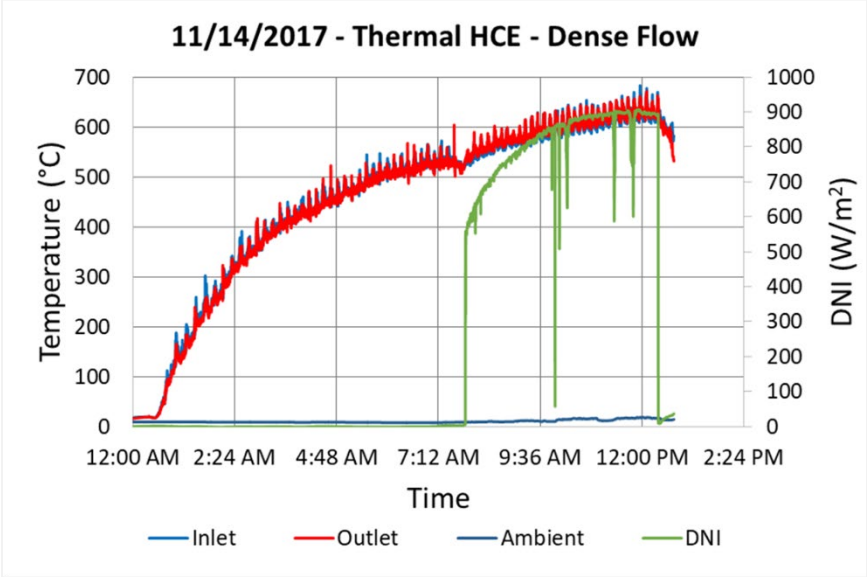

HCE = heat collector element

Based on the 5 kWth STTS system design and test results, the project team also developed a system performance model, a technology-to-market plan, a detailed techno-economic analysis, value-chain mapping, market analysis, and a technology transition plan.

Objectives

The objectives of this project were to:

1. Validate the technology's capability to deliver robust and reliable operation across a diverse range of industrial process heating applications.
2. Achieve a minimum 10 percent increase in fuel efficiency for process heating by effectively integrating high-temperature thermal energy from the STTS system into the existing processes.
3. Provide operational flexibility to accommodate real-time variations in facility process heat demands, ensuring the system can meet changing requirements efficiently.
4. Demonstrate the cost-effectiveness of the STTS technology by achieving a payback period of less than five years, showcasing the economic benefits of implementing the system.

These objectives highlight the project's focus on verifying the technology's performance, efficiency gains, operational adaptability, and economic viability, all of which are crucial factors for successful deployment and adoption of the STTS system in industrial settings. The objectives were to be achieved by scaling up the STTS technology to a full-scale nominal 50 kWth collector with matching particle TTS system, testing the collector on-sun at UCM, the particle TTS system at GTI, and testing the combined system on-sun at UCM.

CHAPTER 2:
Overall System Design

The task involved designing the overall system, comprising a full scale (17-meter [m] long) high-intensity solar collector and the particle TTS system. The nominal rating of the collector was 50 kWth. The system was designed for integration with the existing gypsum kettle at the USG Corporation (USG) field test site. The integration enhances its thermal energy and increases gypsum output. The vertically oriented kettle is housed in a multi-level building.

In the design layout, as illustrated in Figure 8, the collector was positioned in the open outdoor space adjacent to the kettle building, maintaining a clearance of approximately 20 feet (ft) for the passage of USG equipment, materials, and vehicles. The particle hoppers were situated on the third level in the kettle building, in proximity to the kettle. For the particle to process heat exchange, a stainless steel u-shaped tubular heat exchanger (HX) was designed. The HX was designed to be inserted from the top of the kettle, allowing direct contact of the HX surface with the gypsum material as it moves inside the kettle.

The success criteria set by USG included the following:

1. Increase kettle throughput without additional natural gas input.
2. Eliminate external particle venting.
3. Minimize indoor particle venting.
4. Ensure no adverse impacts on kettle performance.
5. Prevent leaks of hot particles.

Figure 8: Placement of the two-stage collector in relation to kettle

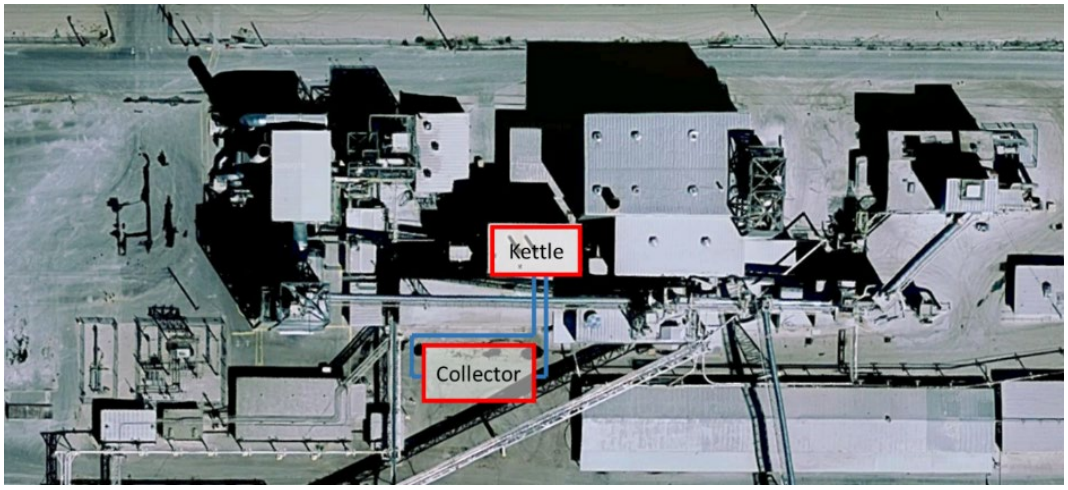

Source: Google Maps, UCM

The conceptual design phase involved the development of the collector and particle TTS system, including the identification of process heating equipment suitable for retrofitting. The

layout of the key components of the system, such as the collector and hoppers, was developed to position these strategically, considering the routing of thermal media piping and the method of introducing thermal energy into the process. Additionally, a comprehensive system heat balance was conducted to ensure optimal performance.

In the existing setup, a single 30-million British thermal units per hour (Btu/hr) burner serves as the heat source for the kettle. Figure 9 illustrates the burner, which generates a firebox temperature of 2,000 °F (1,093.3 °C). The burner uses flue gas recirculation to control nitrous oxide emissions and minimize potential hot spots on the steel sheet separating gypsum from the combustion zone.

Figure 9: Bottom of the gypsum kettle at USG showing the burner

Source: USG

The particle TTS system comprises storage, receiving, and lock hoppers, ensuring a continuous flow of particles through the collector for storage and/or for the process. It was decided to place the receiving and lock hoppers on the third level of the building (Figure 10), adjacent to the kettle, and place the feed hopper near the collector for efficient particle supply.

Figure 10: Space on the third level of building housing the kettle

Source: USG

CHAPTER 3:
High Intensity Solar Collector

Two-stage collector

The design of the full-scale collector is illustrated in Figure 11. It consists of a primary parabolic mirror that tracks the sun and directs sunlight toward the receiver. The receiver, housed within an evacuated glass tube, incorporates a secondary reflector and an absorber. The secondary reflector enhances the concentration of sunlight onto the absorber, resulting in a total concentration of 53 times (7 m / (42 mm x π)). The design of the secondary reflector and the receiver were revised from the earlier one-meter-long versions to increase solar energy capture per unit length, improve heat flux uniformity on the absorber tube and bring the receiver significantly closer to the primary reflector. This reduced the complexity of the receiver support structure and made it easier to focus radiation from the primary reflector onto the receiver, maximizing its intercept factor (ratio of energy from the primary reflector intercepted by the receiver).

Figure 11: Two-stage collector achieves 53x on the absorber

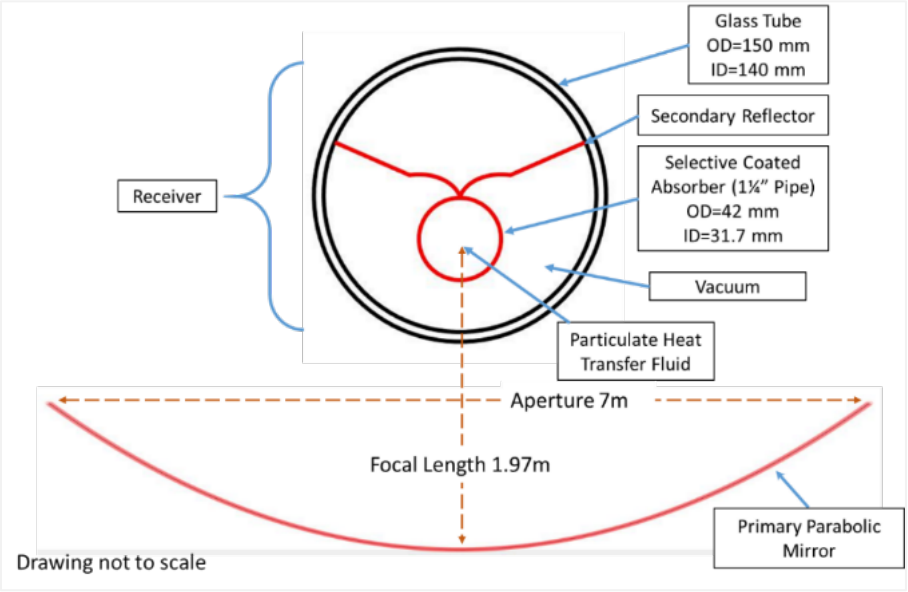

The reduction in distance between the primary reflector and the receiver is evident when comparing the 5 kWth system with a five-meter-wide by one-meter-long primary reflector shown in Figure 6 with the scale drawing of the sideview of the 7-meter-wide by 17-meter-long primary reflector shown in Figure 12.

Figure 12: Side view of the 17-m long collector to scale

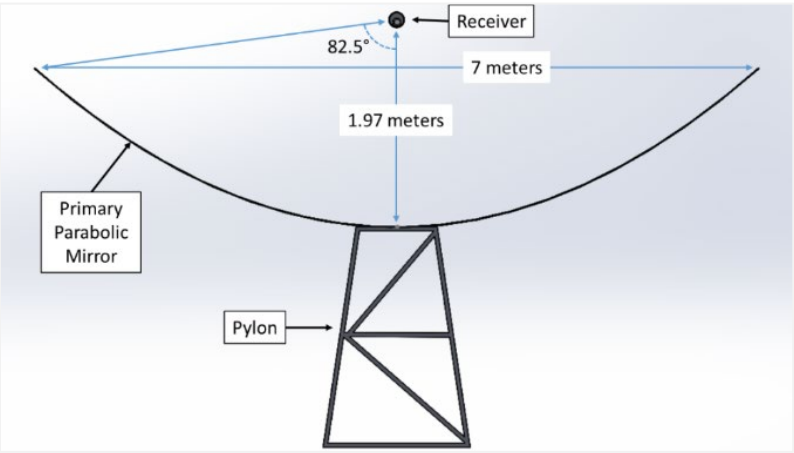

Collector fabrication and testing

For the construction of the receivers, a total of 20 selectively coated absorber tubes, each measuring four meters in length, along with the corresponding glass tubes featuring metal-glass sealed end caps, were acquired. Figure 13 shows an assembly drawing of the receiver, along with an exploded view showcasing its individual components. In Figure 14, the design of the endplate and the positioning mechanism is illustrated. The endplates were machined at UCM.

To optimize reflectance towards the absorber, the secondary reflector was crafted from 316 stainless steel and coated with an aluminum physical vapor deposition (PVD) mirror coating on its reflective side. The back side of the secondary reflector was coated with a black PVD coating to enhance heat dissipation and reduce its temperature.

The absorber tube, also made from 316 stainless steel, was coated on its exterior with a selective low-emissivity coating suitable for high-temperature environments. This coating helps in maximizing the absorption of solar energy by the absorber tube.

Figure 13: Assembly view and exploded view of receiver components

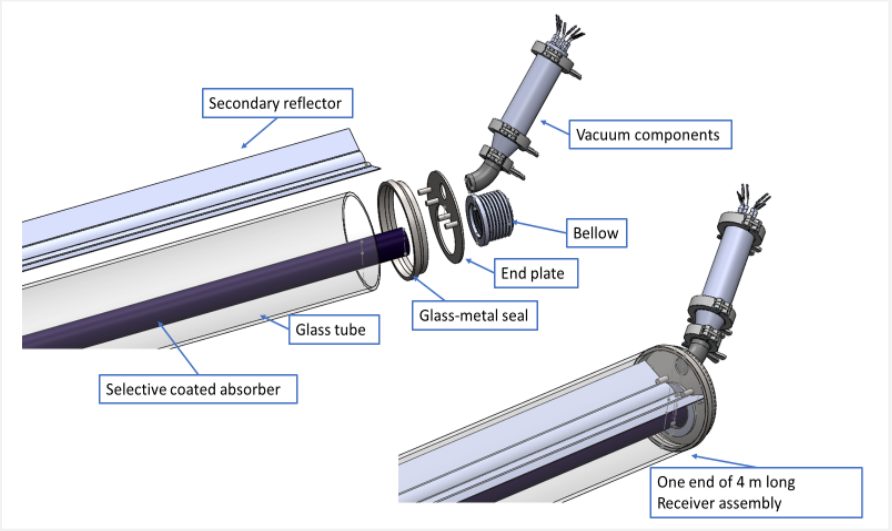

Figure 14: The endplate design and the positioning mechanism for secondary reflector to the endplate

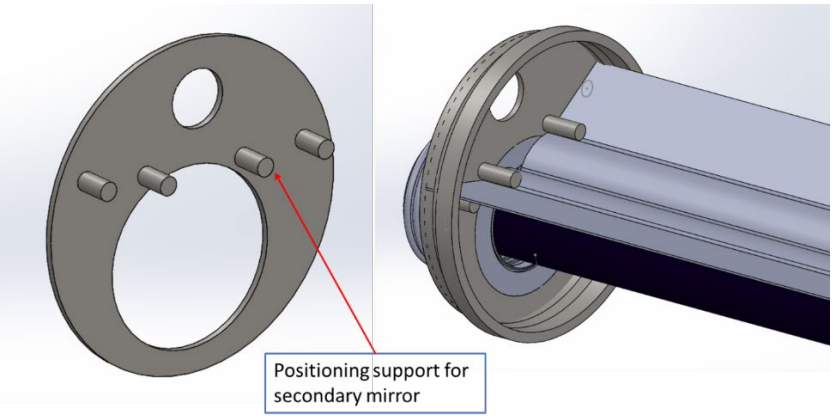

100-hour receiver test at 1,202 °F (650 °C)

After assembling a four-meter-long absorber, a test setup was prepared to facilitate examination of the receiver performance when the absorber was subjected to a temperature of 1,202 °F (650 °C). Figures 15 and 16 show the test setup featuring the receiver.

Two, four-meter-long resistance heating elements, were installed inside the absorber tube to heat the absorber. The temperature of the absorber was regulated by modifying the voltage applied to the heating elements. This allowed precise control and adjustment of the absorber temperature during testing.

Figure 15: 100-hour test s–tup – receiver

Source: UCM

Figure 16: 100-hour test s–tup - vacuum pumps, voltage controller, and data acquisition system

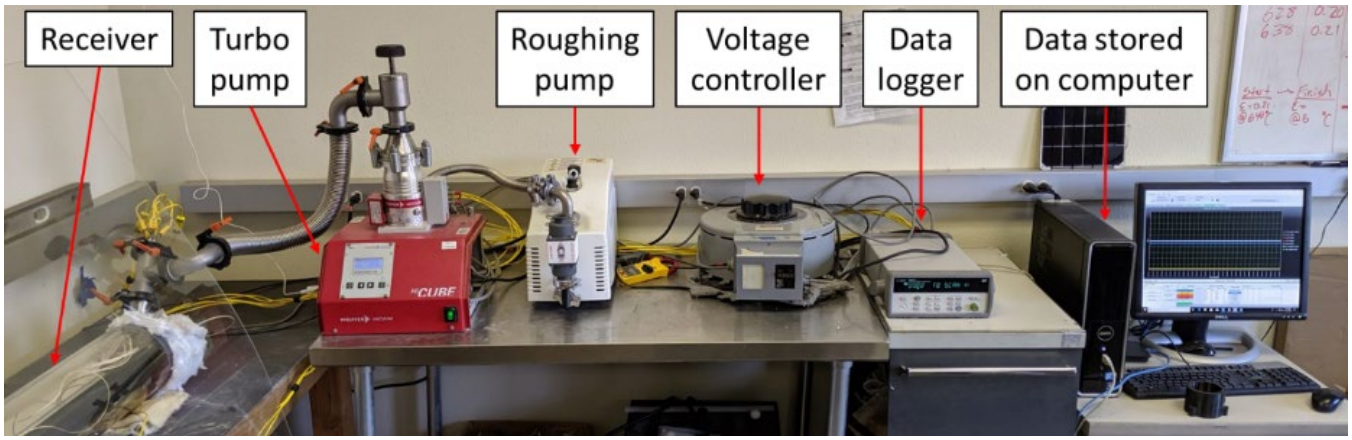

Source: UCM

The absorber temperature was incrementally raised during the test, starting at 572 °F (300 °C), then progressing to 842 °F (450 °C), and finally reaching 1,202 °F (650 °C). Throughout this process, the level of vacuum in the space between the absorber and the glass tube was closely monitored at each temperature. This was done to ensure that outgassing did not cause a reduction in vacuum that could potentially damage the low emissivity coating on the absorber when exposed to high temperatures.

During the test, it was observed that the absorber exhibited bending as its temperature increased to 1,202 °F (650 °C). Further investigation revealed two contributing factors: insufficient expansion-contraction range of the bellows and off-axis placement of the heater within the absorber. These factors resulted in excessive force exerted on the absorber as it heated up, as well as uneven heating around its circumference.

To address these issues, the bellows were redesigned to increase their expansion-contraction range and were also pre-compressed before assembly. This allowed greater expansion, thereby reducing the compressive reaction force exerted on the absorber tubes. Additionally, spacer pins were installed around the electric heater tube to ensure its proper alignment with the tube axis, enabling uniform circumferential heating of the absorber tube. These improvements significantly decreased bending of the absorber tube, maintaining a 10-millimeter (mm) gap between the absorber tube and the glass tube at its maximum temperature.

Subsequently, the absorber was heated and maintained at 1,202 °F (650 °C) for a duration of 100 hours, during which the temperature of its components were continuously monitored. As shown in Figure 17, the absorber tube exhibited a red glow at this temperature.

Figure 17: Receiver undergoing 100-hour testing at 1,202 °F (650 °C)

Source: UCM

Figure 18 illustrates the temperatures recorded for the absorber, the secondary reflector, and the surface of the glass tube at the top and bottom sections. Additionally, it presents the emissivity of the absorber throughout the 100-hour test period. It is worth noting that no significant deformation of the receiver components was observed during the test. Upon cooling, the bellows returned to their original pre-compressed length, confirming the effectiveness of the two-way precompression approach.

Figure 19 shows the variation of surface emissivity with the absorber temperature over the course of the 100-hour test. The emissivity at the beginning of the test was measured to be 0.19, which gradually increased to approximately 0.24 and then remained stable for the remainder of the test duration. Based on a direct normal irradiance value of 1,000 watts per square meter (m2) on the primary reflector, the estimated radiation loss amounted to 146 watts/m2 or 14.6 percent.

Figure 18: 100-hour heating test results

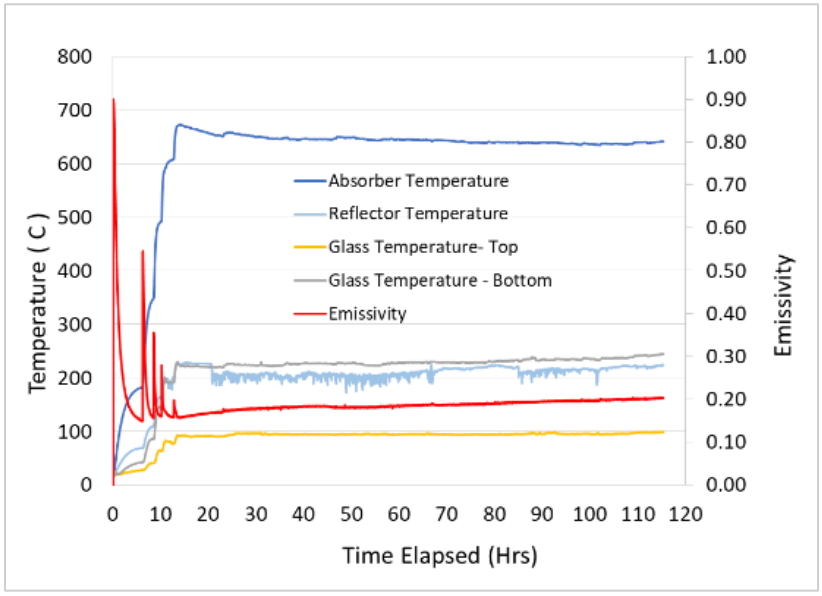

Figure 19: 100-hour test results - absorber surface temperature and emissivity

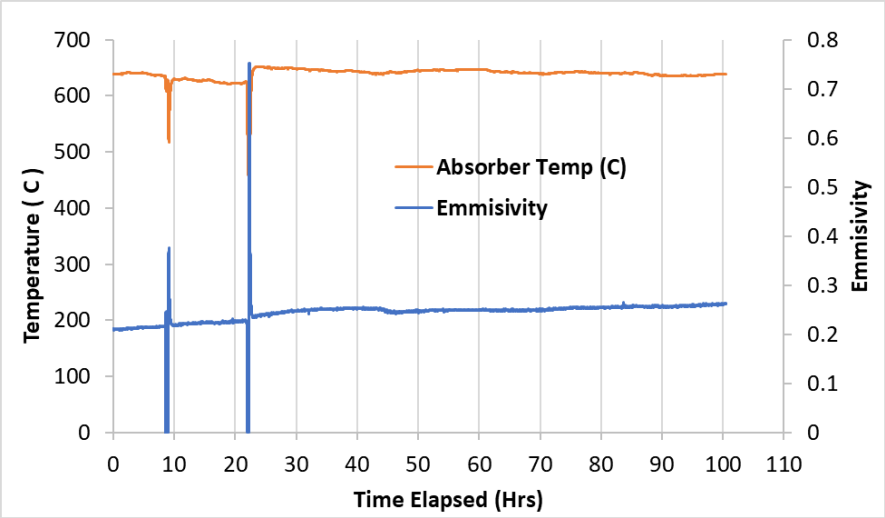

Parabolic collector installation

After successful completion of the 100-hour test, an additional set of four, 4-meter-long receivers were assembled and various components necessary for the assembly of a commercial parabolic trough module (shown in Figure 20) were procured. These components included pylons (legs), a hydraulic drive motor for tracking purposes, a space frame, parabolic ribs, mirror panel tracks, receiver support mounts, and space frame nodes.

To facilitate installation both at UCM and later at the host site, a skid-mount was designed and constructed for the collector system. This design eliminated the need for below-ground concrete piers typically required for parabolic trough installations, along with the associated permits.

Due to the unavailability of the original mirror panels from the manufacturer, new mirror panels were fabricated using stainless steel material. These mirror panels were equipped with a laminated reflective film called ReflectechR, as shown in Figure 21.

Figure 20: Parabolic trough module with labelled components

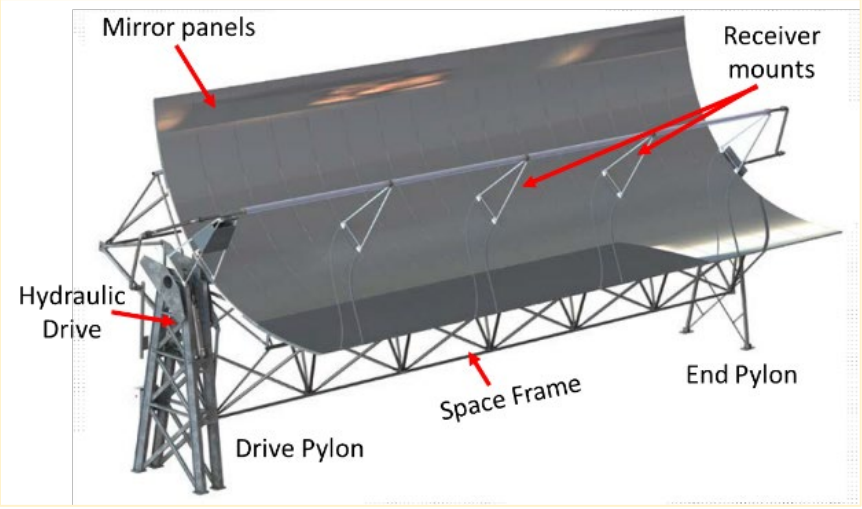

Figure 21: Mirror panel lamination

Source: UCM

Figures 22, 23, and 24 show the installation progression of the parabolic collector at UCM. The parabolic mirror frame was assembled and tested for rotation, followed by installation of the mirror panels.

Figure 22: The mirror support space frame assembled and rotated at UCM

Source: UCM

Figure 23: Installation of first half mirror panel on the parabolic ribs

Source: UCM

Figure 24: Parabolic trough with absorber support structures installed at UCM

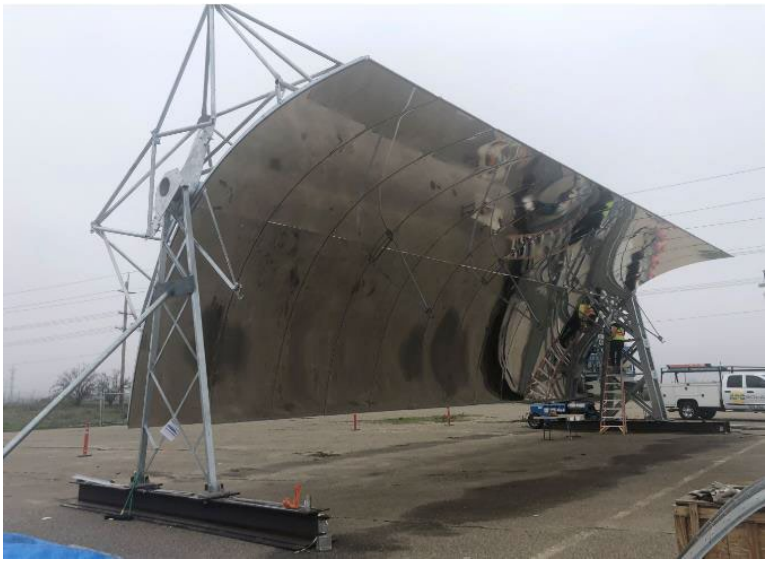

Source: UCM

Four-meter-long receivers

Figure 25 shows the four, 4-meter-long receivers that were specifically fabricated for on-sun testing. As part of the quality control process, all tubes underwent a leak check, and no leaks were detected during the test conducted at a 10-7 cubic centimeters per second helium leak rate detection setting.

Among the four receivers, two units used a 6.5 mm inner diameter copper tubing for the vacuum port, while the other two employed a 25 mm standard KF flange. The decision to use the smaller diameter copper tube was to enable crimp-sealing using a custom-designed tool once the desired vacuum level was achieved. This approach ensured effective sealing of the tube while maintaining the necessary vacuum conditions.

Figure 25: The four assembled receiver tubes

Source: UCM

On-sun optical efficiency tests

After installation of the parabolic trough was completed, a dummy absorber tube was mounted to evaluate the mechanical and optical performance of the mirrors and to ensure proper alignment of the absorber. The dummy absorber tube was a nominal 2.5 inches schedule 40 steel pipe with an outer diameter of 73 mm. To maximize radiation absorption, the tube was coated with black paint.

Figure 26 shows the parabolic mirror along with the dummy absorber tube (referred to as the receiver tube in the figure) during on-sun testing. This setup allowed for comprehensive testing of the primary reflector's optical properties and the alignment of the absorber tube.

Figure 26: On-sun optical testing using 73 mm diameter dummy absorber tube

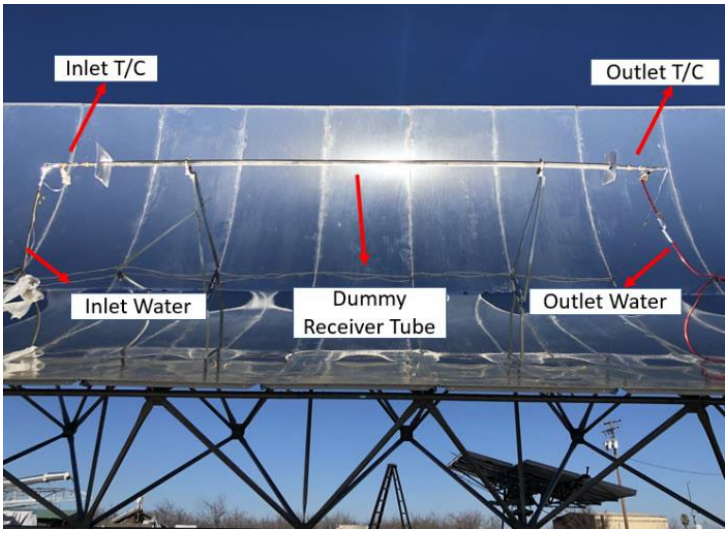

Source: UCM

The bare dummy absorber tube, when tested with water flowing through it at a rate of 350 gallons per second (in the turbulent flow regime), resulted in a temperature rise of 57.2 °F (14 °C). Based on this temperature rise and flow rate, the solar to thermal efficiency was determined to be 62 percent. However, during the testing, it was observed that the bare dummy absorber tube had developed an upward bend, as shown in the top photograph of Figure 27.

This is believed to be a result of stratified flow of water within the 73 mm dummy absorber tube, which caused a non-uniform circumferential temperature distribution, leading to the bending of the absorber tube. The bending further reduced the solar intercept factor and radiation flux on the tube resulting in efficiency loss. This observation aligns with the results obtained from the optical simulation depicted in the bottom graphics in Figure 27.

It was expected that the use of a smaller diameter (42 mm) absorber with the secondary reflector would eliminate non-uniform illumination and stratified flow; thereby, reducing most of the bending of the absorber tube and significantly increasing the intercept factor. Additionally, the glass tube with vacuum surrounding the actual absorber tube, along with its smaller surface area, would help mitigate convective losses. These improvements were anticipated to result in a substantial increase in optical efficiency.

Figure 27: Results of optical simulation to estimate reduction in intercept factor due to upward displacement of absorber during on-sun testing

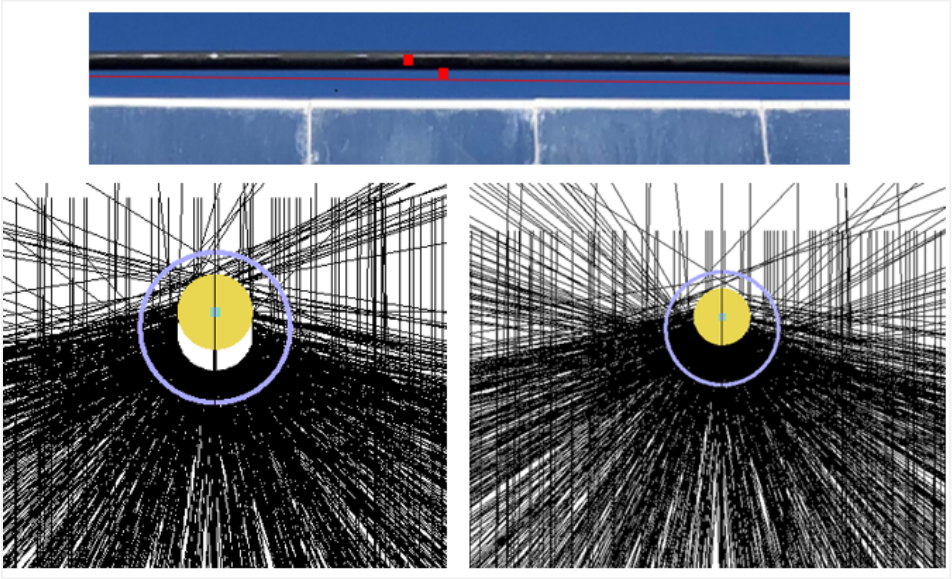

Source: UCM

After conducting testing with the dummy absorber tube and intercept factor assessment using ray tracing, three out of the four receivers mentioned previously were installed onto the absorber tube supports within the primary parabolic reflector for on-sun optical testing. Since the original mounting brackets that came with the primary reflector were designed for 80 mm outer diameter absorber tubes, new brackets were specifically designed and fabricated to accommodate the smaller 42 mm outer diameter high absorber used in the current system. Figure 28 illustrates the assembled system undergoing on-sun testing.

Figure 28: On-sun optical testing of three, 4-meter-long prototype receivers at UCM

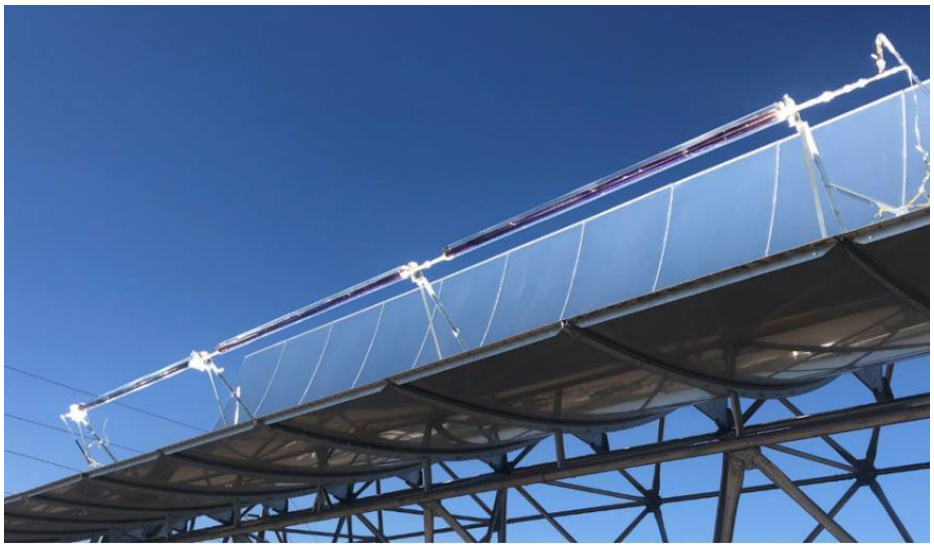

Source: UCM

Figure 29 displays the measured solar input, thermal output, and the corresponding efficiency values. The recorded optical efficiency of 55 percent was significantly below the design value of about 70 percent. This discrepancy is attributed to several factors:

1. Bubbling of the PVD aluminum coating on the secondary reflector.
2. Outgassing from the secondary reflectors and subsequent deposition on the glass tubes.
3. Warping and waviness observed in the stainless steel secondary reflectors.

Figure 29: Optical efficiency test results

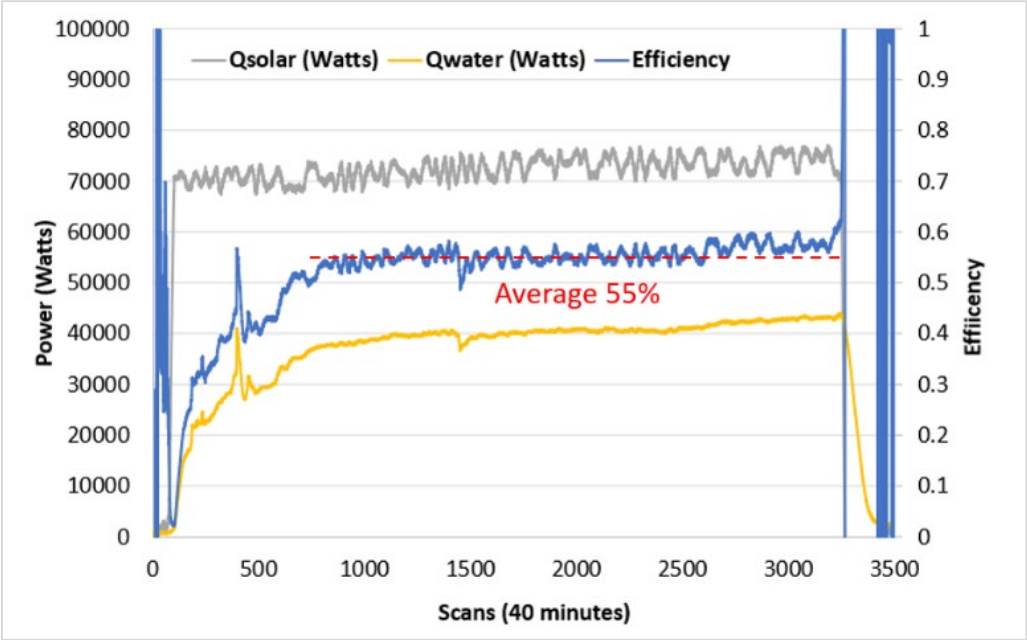

To address these issues, the design, material, and assembly process of the secondary reflector were revised. The new reflectors were constructed using commercial Alanod mirosilver sheets, which feature a silver coating on an aluminum base metal, instead of the previously used laminated stainless steel sheets. The two wings of the reflector were joined together using rivets, in contrast to the previously used welding method. Additionally, a high-temperature ceramic black coating was applied to the back of the secondary reflector to enhance emissive cooling and minimize the potential for warping. The team anticipated that these modifications, along with the higher reflectance (97 percent as per the manufacturer) of the Alanod material and the significantly higher thermal conductivity of aluminum compared to stainless-steel, would prevent overheating of the secondary reflector, and improve its temperature uniformity. Figure 30 shows the modified receiver tubes featuring the new aluminum secondary reflectors. Three new receivers were constructed and mounted for on-sun optical efficiency testing, as shown in Figure 31. During this test, each tube was connected in series with vacuum hoses, and a vacuum pump was employed to remove any outgassed materials. The team expected improved optical efficiency compared to the previous tests conducted with stainless steel secondary reflectors.

Figure 30: Receiver assembly with new aluminum secondary reflectors

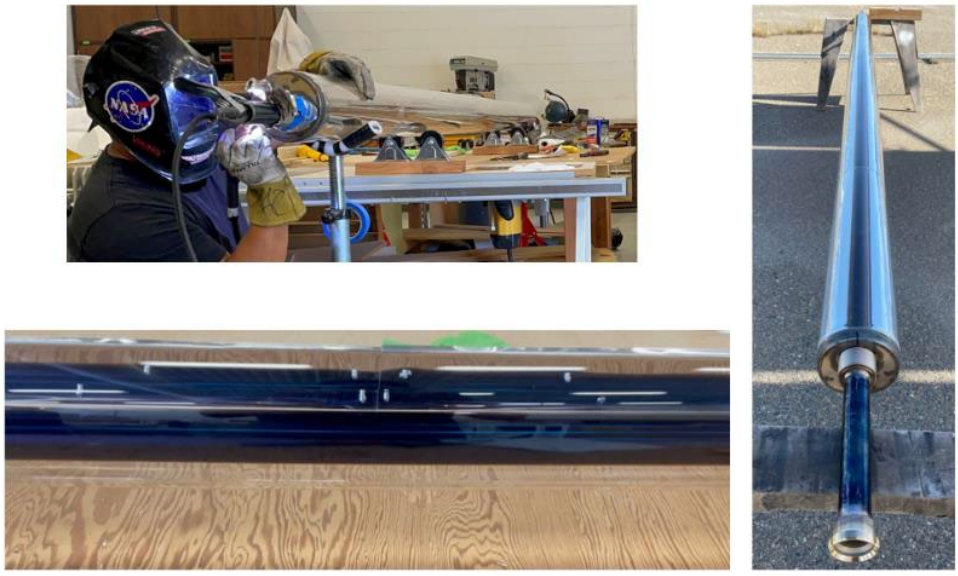

Source: UCM

Figure 31: Three, 4-meter-long receivers with new secondary reflectors mounted for on-sun optical efficiency testing

Source: UCM

The revised secondary reflectors successfully resolved many of the issues encountered with the stainless steel versions. No instances of outgassing, bubbling of the coating, or warping of the secondary reflectors were observed. The glass tubes on the receivers remained intact without any breakage. However, the issue of absorber tube bending and the associated losses due to gaps remained unresolved. As illustrated in Figure 32, there was no discernible improvement in optical efficiency compared to the earlier receivers featuring stainless steel secondary reflectors.

Figure 32: Optical efficiency results with the Alanod secondary reflectors

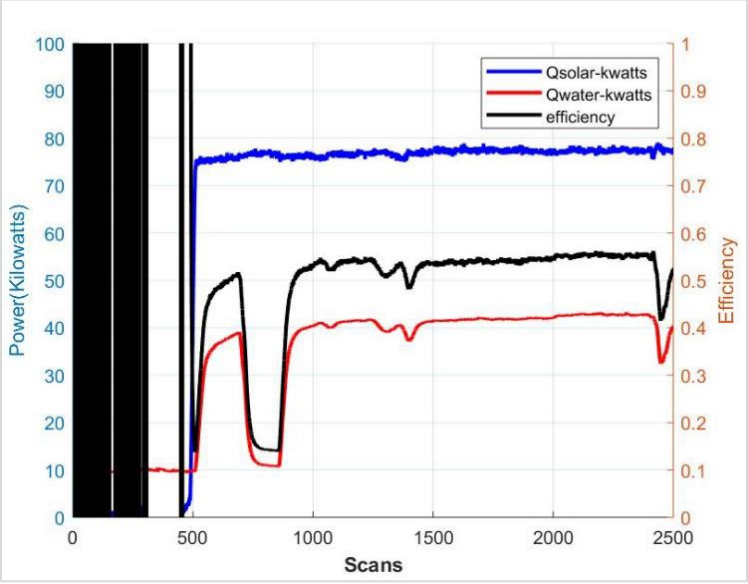

To gain further insight into the thermal conditions at the absorber, thermal and fluid flow simulations were conducted using COMSOL Multiphysics (software) finite element analysis. The model incorporated solar radiation fluxes obtained from the optical model (Figure 33) and applied these as thermal boundary conditions on the absorber tube. The simulations were

performed for different water flow rates to analyze the temperature distribution around the absorber tube, as depicted in Figure 34. Here, the right X axis shows the temperature distribution along the right circumference of the absorber and the left X axis shows the symmetrical left circumference temperature distribution.

The results revealed that the two-stage high intensity absorber exhibited a significantly more uniform flux distribution compared to single-stage absorbers, which should provide a more uniform circumferential temperature distribution on the absorber. At a water flow rate of 0.85 kilogram per second (kg/s), equivalent to 3500 watts per square meter per kelvin (W/m2K), the peak and valley circumferential temperature gradient was found to be less than 41 °F (5 °C). However, in the tests conducted thus far, the flow rate through the receivers was limited to 0.2 kg/s to 0.3 kg/s due to the constraints of the city water line, resulting in a temperature gradient exceeding 41 °F (5 °C).

Figure 33: Ray tracing and radiation flux distribution around the high intensity absorber

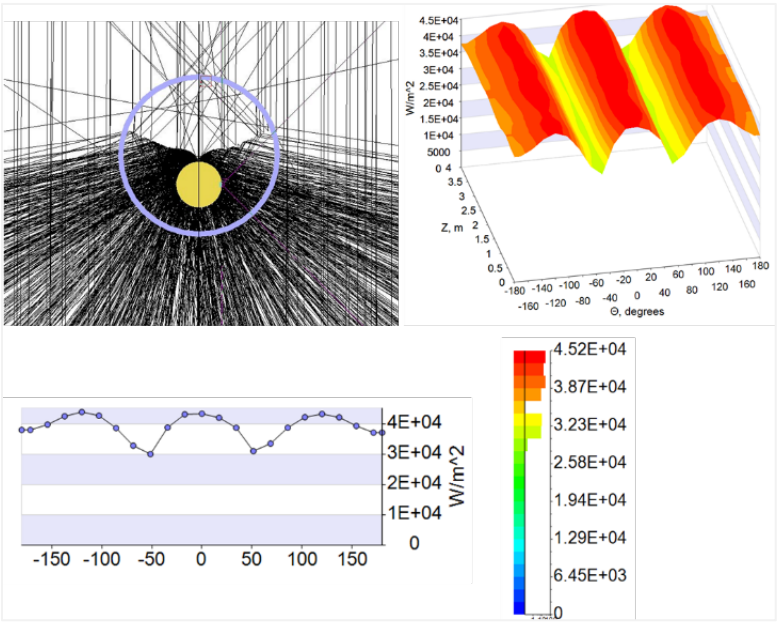

Figure 34: The thermal and flow analysis of the 42 mm high intensity absorber

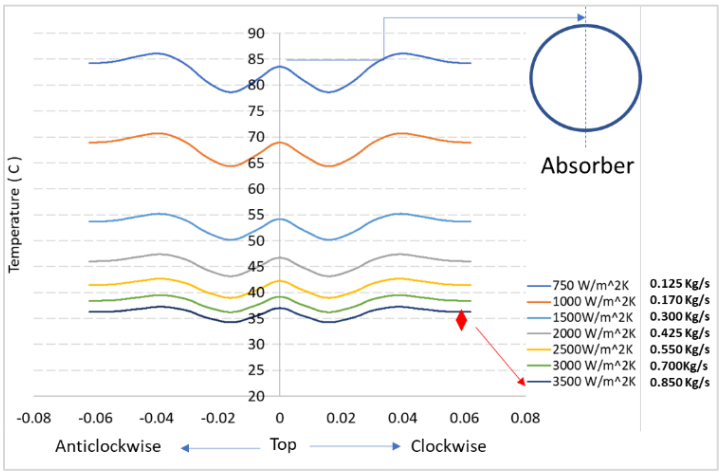

To assess the impact of secondary reflector rotation and absorber displacement on the intercept factor, a ray tracing optical analysis was conducted as illustrated in Figure 35. This analysis aimed to evaluate the potential loss in the intercept factor resulting from the movement of these components during operation and tracking.

By simulating the rotational movement of the secondary reflector and the displacement of the absorber, the analysis provided insights into the changes in the intercept factor under varying conditions. The results of this analysis provided better understanding of the potential losses in solar energy collection efficiency due to these movements, thus informing further design considerations and optimization strategies.

Figure 35: Optical analysis of the secondary reflector and the absorber

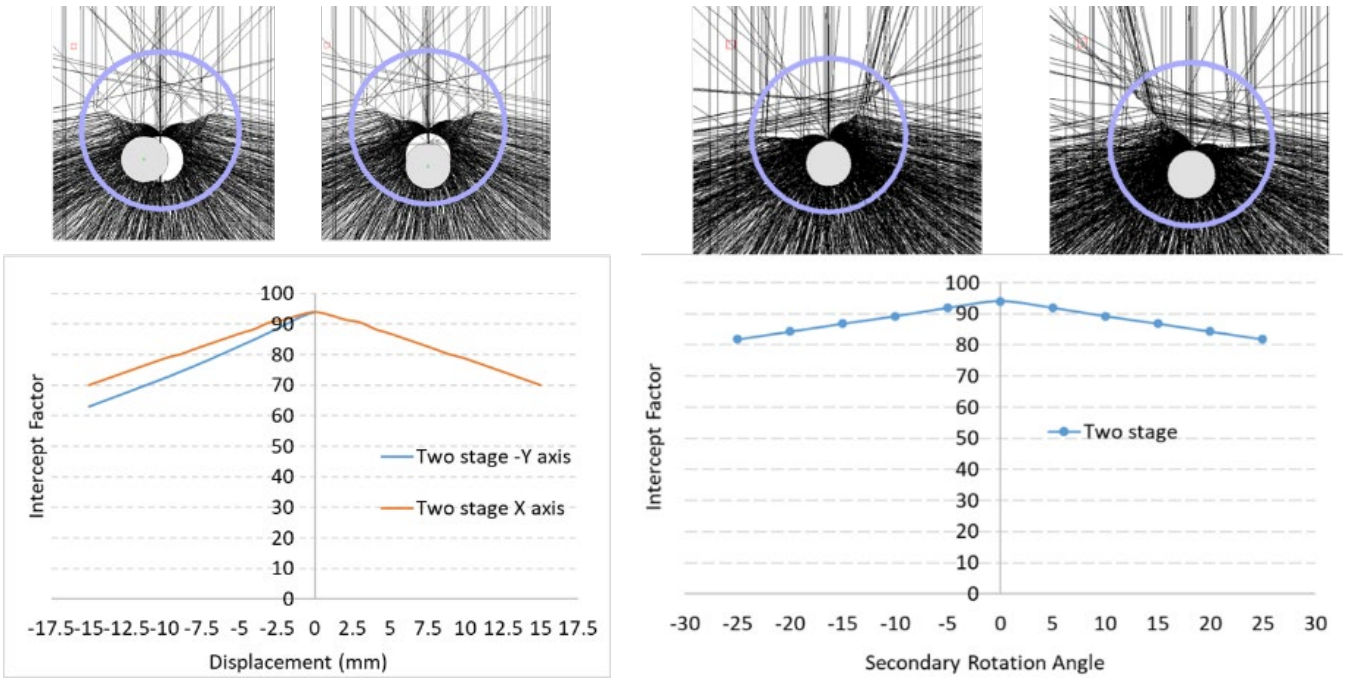

To address the issues related to absorber tube bending and improve the overall performance of the STTS system, the research team decided to focus on modeling the receiver and conducting front-end engineering. Modeling aimed to analyze and optimize the thermal behavior of the receiver, address factors contributing to absorber tube bending, while the front-end engineering activities would help refine the design and identify any other operational or design-related issues.

The modeling efforts involved the implementation of analytical and numerical models to simulate the thermal behavior of the receiver. Various input parameters, such as absorber temperature, material properties, wall thickness, length, heat transfer fluid properties, and flow rate were considered in the model. By running multiple cases with different input values, the team aimed to understand the impact of these parameters on absorber bending and thermal efficiency.

Simultaneously, front-end engineering activities were undertaken, starting with conceptual engineering, and progressing to preliminary engineering to refine the design and estimate

costs. This process culminated in the development of a generic 2 MWth size reference plant design. The engineering assessment was also designed to identify and address any other design or operational challenges associated with the STTS equipment.

By combining modeling and front-end engineering efforts, the research team addressed the absorber bending issues and provided a solid foundation for future demonstration and commercialization of the STTS technology. This approach enabled optimization of the system's performance, refining the design, and enhancing potential for successful deployment of the STTS technology.

Self-consistent model

Figure 36 illustrates the architecture of the model developed to address the thermal behavior and deformation of the receiver in the high-temperature solar collector. The model consists of three interconnected modules: illumination, thermal behavior, and deformation analysis.

The illumination module uses previously implemented tools to calculate the surface irradiation of the absorber. It provides the distribution of solar flux on the absorber surface based on longitudinal and circumferential positions.

The thermal behavior module incorporates a conjugate heat transfer model. It considers conduction within the absorber wall, convection to the heat transfer fluid, and radiative heat loss. The module takes the surface solar flux distribution from the illumination module as input and predicts the average wall temperature as a function of longitudinal and circumferential positions.

The deformation module focuses on predicting the deformed shape of the absorber. It applies a discretized one dimension bending approximation that accounts for the non-uniform thermal strain, gravitational loading, and constraints. The module predicts the lateral displacement of the absorber as a function of longitudinal position.

The updated geometry obtained from the deformation module is fed back to the illumination module, and the entire model is iterated until a self-consistent equilibrium geometry is achieved for the given operational conditions. This iterative process ensures that the absorber's deformation, temperature, and surface illumination values are consistent with each other.

Figure 37 illustrates the maximum absorber deformation under representative operational conditions. It provides insights into the effects of high temperature with particle suspension flow and ambient temperature with water on the deformations observed in the absorber.

By integrating these modules and iterating until convergence, the model enabled exploration of meaningful parameter spaces related to operational, design, and material parameters. This allowed for a comprehensive analysis of the thermal behavior, deformation, and efficiency of the high-temperature STTP system.

Figure 36: Integrated receiver model architecture

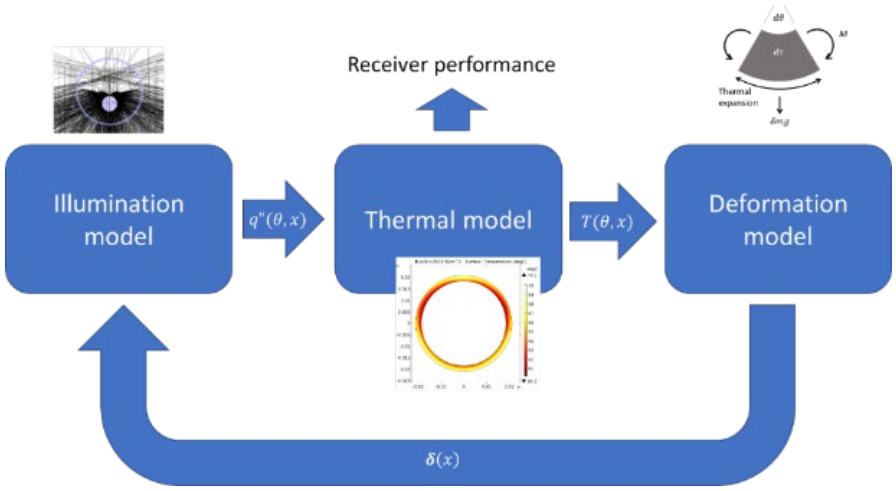

Figure 37: Maximum deflection of absorber (at longitudinal center) vs. total free absorber span for: a) particle suspension, 1,202 °F (650 oC) inlet, 0.277 kg/s flow rate; and b) water, 86 °F (30 oC) inlet, 0.48 kg/s flow rate

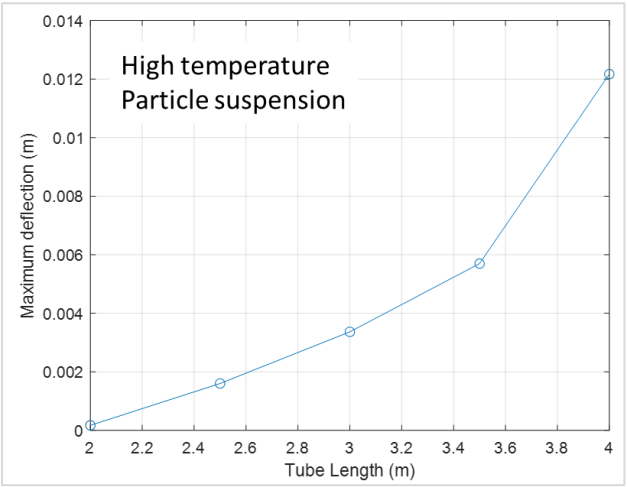

(a)

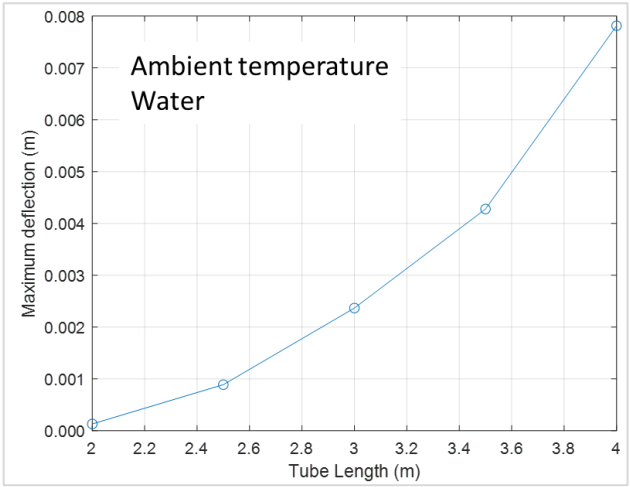

(b)

The illumination module in the model used a two-dimensional ray tracing algorithm implemented in Python. Figure 38 provides a schematic representation of a simulated absorber arrangement. The arrangement consists of a large parabolic mirror that serves as the primary reflector, and a secondary reflector positioned above it. The absorber tube, according to the design, is placed directly below the secondary reflector.

In the schematic, the incoming rays from the sun are depicted with an appropriate angular spread. These rays are shown striking the parabolic reflector, with the focal point located at coordinates (0,0), and a focal length of two meters. The purpose of the ray-tracing algorithm is to track the paths of these rays and determine their interactions with the primary reflector and receiver components.

By simulating the ray paths and calculating the distribution of solar flux on the absorber surface, the illumination module provides valuable information regarding the illumination

profile experienced by the receiver system. This information serves as a crucial input for the subsequent thermal and deformation analyses in the model.

Figure 38: Schematic of solar rays incident on/reflected from primary reflector and intercepted by the absorber tube and the secondary reflector

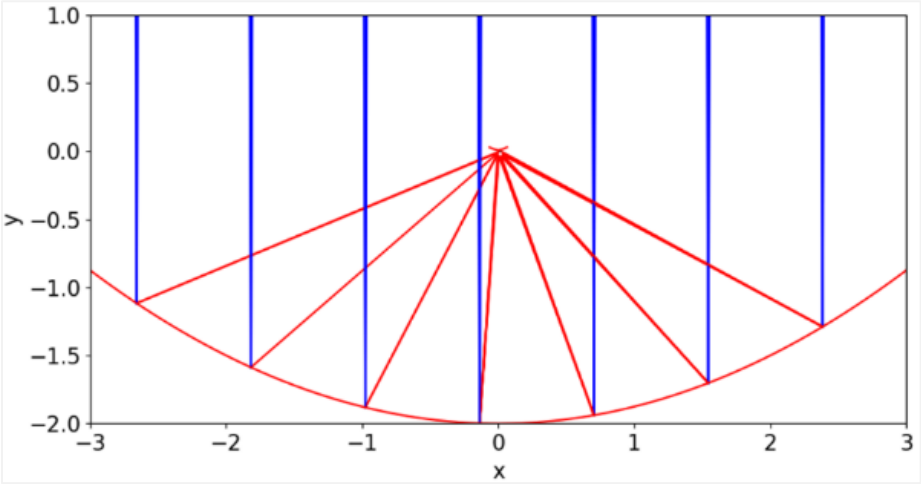

Figure 39 shows schematics of the implemented ray-tracing algorithm. An arbitrary incident ray (Figure 39a) is reflected by any reflecting plane. The angle of incidence is equal to the angle of reflection with respect to the normal.

If $\vec{p}$ denotes the incident ray, then $\vec{r}$, the reflected ray bounced back from a reflecting plane with unit normal, $\hat{n}$ can be written as:

$$\vec{r} = \vec{p} - 2(\vec{p} \cdot \hat{n})\hat{n} \quad (1)$$

An absorber with center (a_x, a_y) and radius r can be represented vectorially as:

$$\|\vec{x} - \vec{a}\|^2 - r^2 = 0 \quad (2)$$

where $\vec{x} = \begin{Bmatrix} x \\ y \end{Bmatrix}$ and $\vec{a} = \begin{Bmatrix} a_x \\ a_y \end{Bmatrix}$. Let, $\vec{q} = (q_x, q_y)$ be the intersection point of the reflected ray and the absorber. To solve for $\vec{q}$, we need to find a unique t_0 such that:

$$\vec{q}(t) = \vec{p} + \mathrm{rt}_0\hat{d} \quad (3)$$

Next, the intersection points on the absorber tube are converted from cartesian to polar coordinates and the illumination flux distribution on the absorber surface (Figure 39b) is accumulated. The algorithm is relatively fast and is independently run for each segment along the absorber length.

Figure 39: Schematic ray tracing algorithm for illumination module. (a) Incident ray reflected from a mirror surface, (b) striking absorber tube after reflection

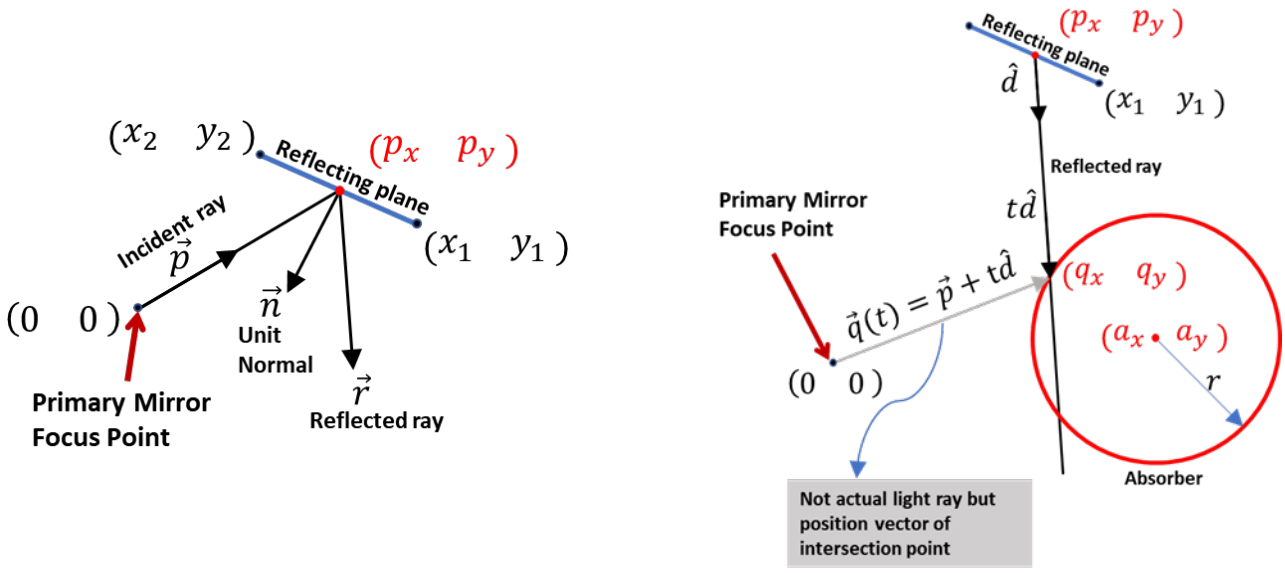

The thermal model within the overall system was developed to predict the temperature profile of the absorber based on the input of illumination flux obtained from the illumination module. This model considers various factors such as radiative heat transfer from the absorber to the surrounding environment, convective heat transfer to the heat transfer fluid, and conduction throughout the solid absorber material.

The algorithm of the thermal model follows a specific procedure to calculate the temperature distribution. It begins with an initial estimation of the temperatures of the fluid and solid components. The process then involves iteratively evaluating the conjugate conduction, convection, and radiation fluxes, and reevaluating the temperatures at intersection points. This iteration continues until the model reaches convergence, meaning that the temperatures have stabilized, and the calculations have achieved a self-consistent solution.

Figure 40 provides a flowchart illustrating the sequence of steps in the thermal model algorithm. It demonstrates the iterative process and the interplay between the various thermal mechanisms considered in the model. By simulating the temperature profile within the absorber, this thermal model contributes to understanding the thermal behavior of the system and provides input for the subsequent deformation analysis.

Figure 40: Algorithm of the thermal model

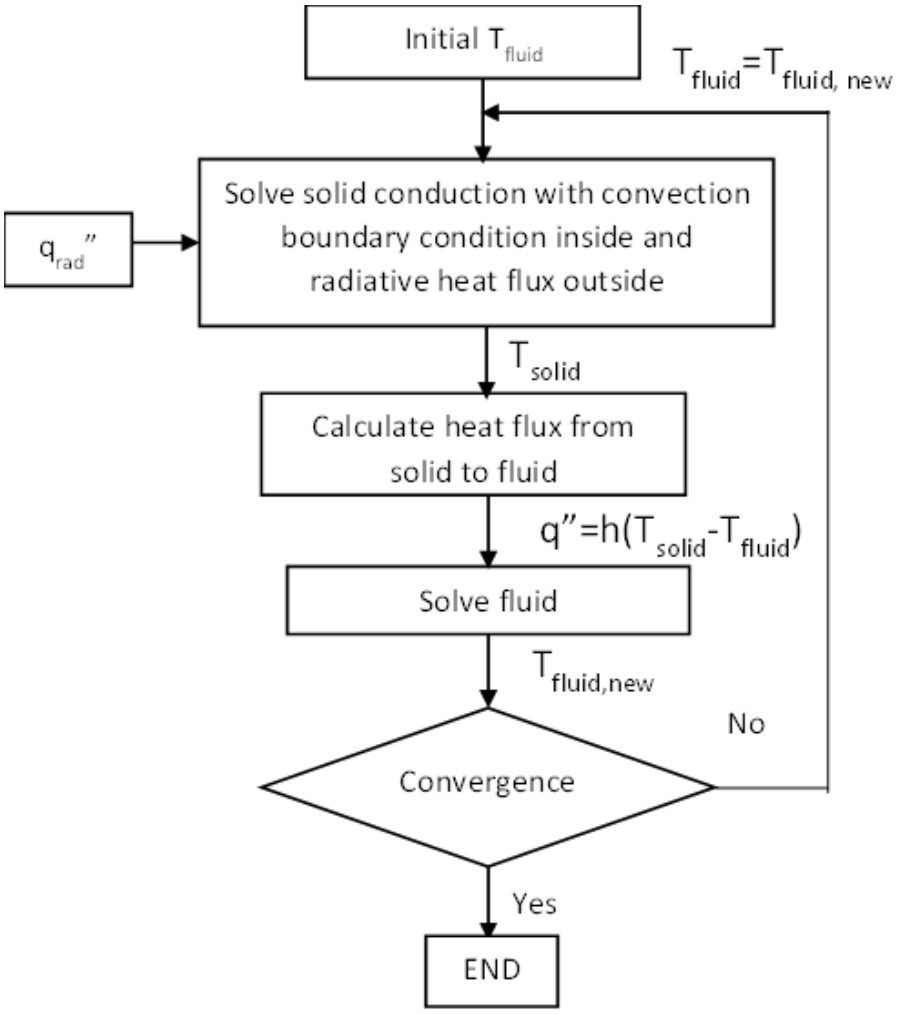

The thermal model uses steady-state equations in cylindrical coordinates to analyze the temperature distribution within the system. The finite difference method is employed to solve these equations numerically for each domain. In the case of the solid domain, it is discretized into a mesh with 40 points along the length of the absorber, 21 points along the circumference, and 3 points through the thickness.

As an example, Figure 41 presents a representative result for a test case where the absorber is not deformed, and water is used as the working fluid. The inlet water is assumed to be at room temperature. The figure displays the temperature distribution within the absorber, with different colors indicating different temperature levels. Additionally, the corresponding heat flux, which represents the amount of heat transferred per unit area, is also depicted.

This representation provides insight into the thermal behavior of the system under the specified conditions, demonstrating the temperature variation within the absorber and the associated heat flux distribution. These results are obtained through the application of the finite difference method and serve as valuable information for further analysis and optimization of the system.

Figure 41: Result of the test case with water as a working fluid, and with the given heat flux input distribution

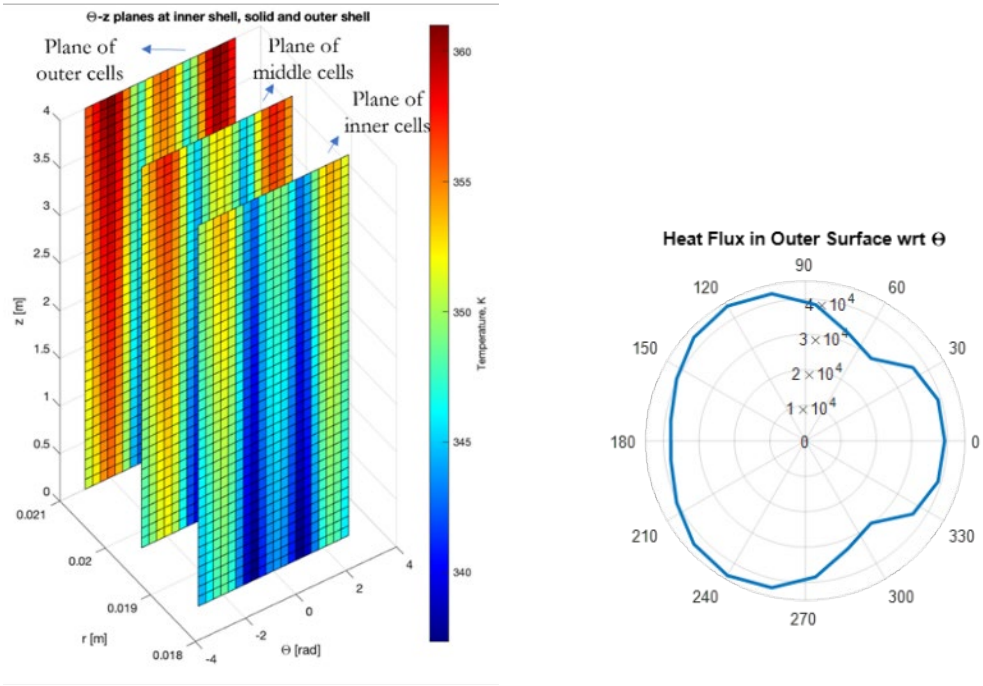

The deformation module employs a linear simple bending member approximation to predict the deformations of the absorber tube. In this model, it is assumed that the absorber tube has a thin annular cross-section throughout the analysis. Figure 42 illustrates a schematic of the discretized absorber tube, considering the gravitational load due to its weight and the simple bending moments developed at each element of the tube.

In the analysis, the temperature distribution T = T(θ, x) along the absorber tube is considered. For a small section of the tube with a length Δx (referred to as a tube element), it is assumed that the temperature distribution T = T(θ) is uniform across the short length and through the thickness but varies around the circumference. It is also assumed that the absorber tube expands only along its axis (x direction).

By considering the non-uniform temperature distribution and the gravitational load, the model predicts the resulting deformations of the absorber tube. This approximation allows for the estimation of the bending and displacement of the absorber tube, considering the thermal effects on its structural integrity.

This simplified approach provides a practical and computationally efficient method for analyzing the deformation of the absorber tube under the given conditions, while accounting for both temperature variations and gravitational forces.

Figure 42: Schematic of the absorber as a simply supported beam subjected to gravitational distributed loads along its length and varying thermal bending moments due to circumferential temperature distribution

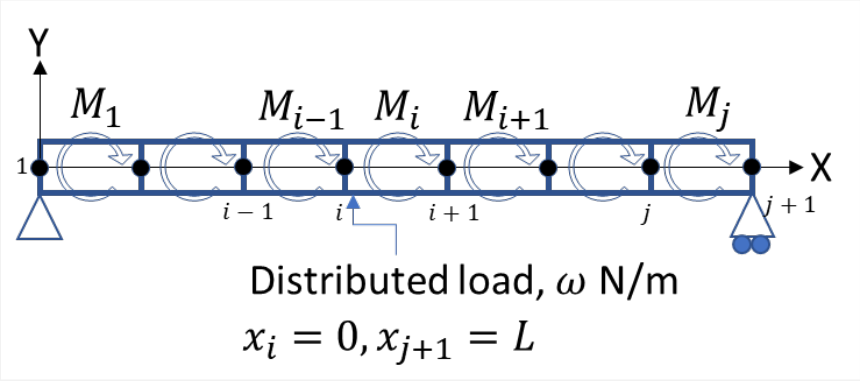

To calculate the thermal deflection of the absorber tube, the effort focused on a small element (i) within the tube. The circumference of the tube was discretized into multiple nodes and elements. Each node stored a temperature value T_(i,θ) and could be represented as a vector with magnitude T_(i,θ) and direction pointing from the center of the absorber to the node along the circumference (θ direction). By considering these temperature vectors, an effective temperature gradient across the cross-section of the tube could be determined, resulting in a simple bending moment within the tube element. The deflection of the absorber tube caused by this bending moment was then calculated for each individual element, as depicted in Figure 43. By applying appropriate boundary conditions and ensuring continuity requirements, the overall deflection along the entire length of the tube could be determined.

Figure 43: Schematic of the deflection of beam due to temperature distribution

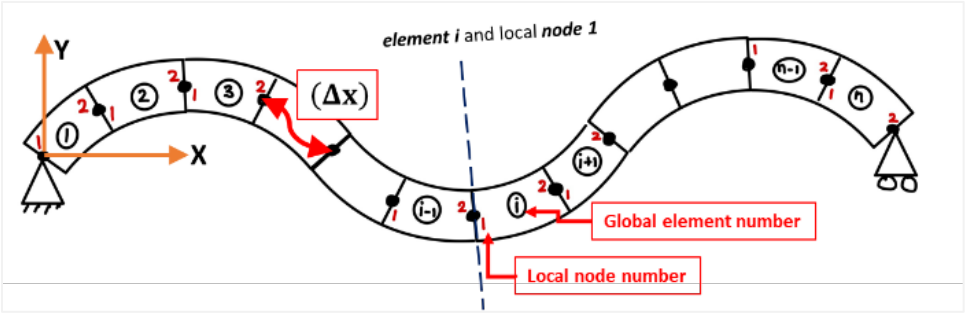

Boundary Conditions:

At $x = 0, L : y = 0$

C^1 continuous at the internal nodes i.e.

$$u_{i2} = u_{(i+1)1} \tag{4}$$

$$\frac{du_{i2}}{dx} = \frac{du_{(i+1)1}}{dx} \tag{5}$$

$$u_{i2} = u_{(i+1)1} \tag{4}$$

$$\vec{u}_{i2} = \frac{\alpha}{2d}(\Delta x)^2\left(\sum_{k=1}^{i}\vec{T}_k - \frac{i}{n}\sum_{k=1}^{n}\vec{T}_k\right) + \frac{\alpha}{d}(\Delta x)^2\left(\sum_{\substack{j=1 \\ j<i}}^{i-1}(i-j)\vec{T}_j - \frac{i}{n}\sum_{j=1}^{n-1}(n-j)\vec{T}_j\right) \tag{6}$$

$$\vec{u}_{n2} = 0 \tag{7}$$

Where $\alpha = 17.3e-6$: co-eff of linear expansion of 304 SS and $n = 40$ is total number of beam elements.

Linearity of the model allows direct superposition of the deformation due to gravity. The governing equation (eq. 8) and the boundary conditions for the distributed gravitational loading follows:

$$\frac{d^2u_{y_2}}{\mathrm{d}x^2} = \frac{0.5}{EI}\omega x(L-x) \tag{8}$$

boundary Conditions:

At $x = 0, L : y = 0.$

The deflection due to gravitational load can be calculated as per eq. 9, and the total deflection is a superposition of the two independent deflections u_{i_1} and u_{i_2} (eq. 10).

$$u_{i_2} = -\frac{\omega}{24EI}(x^3 + L^3 - 2Lx^2)x \tag{9}$$

$$u = u_{i_1} + u_{i_2} \tag{10}$$

Subsequently, the final implementation of the self-consistent model was completed to address absorber deformation under illumination and gravity and the influence on overall receiver performance. Figure 44 shows an overview of the final model.

Figure 44: Overview of self-consistent solar thermal absorber model

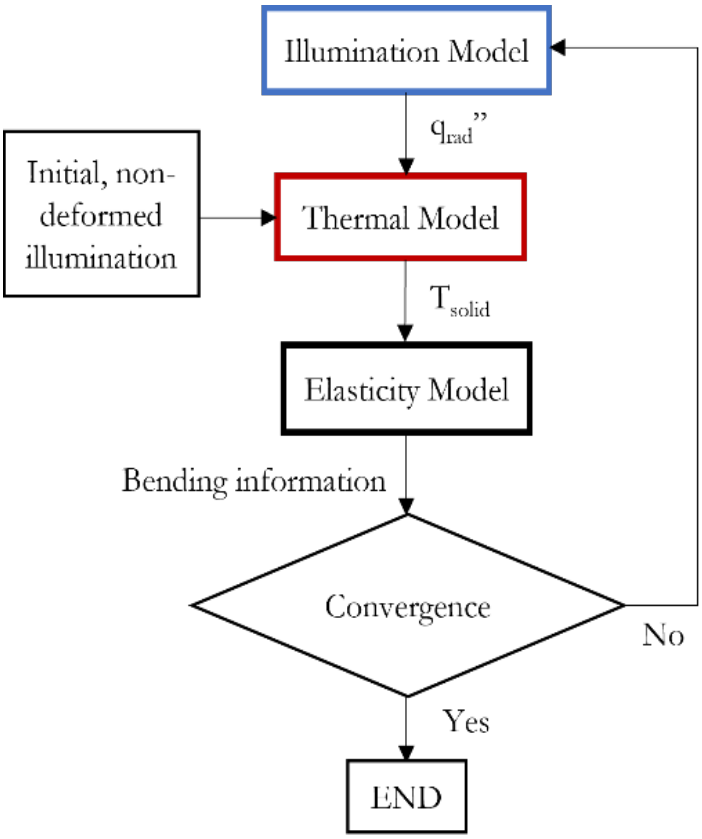

Several enhancements were made to the final illumination model to improve its accuracy. Firstly, the shadow cast by the secondary reflector was incorporated in the model, accounting for approximately 1.8 percent of occluded solar radiation. Secondly, additional factors such as the finite size of the sun's disk, imperfect specularity of the reflectors, and possible pointing errors for the collector were considered in the angular distribution of incident solar illumination. Each component is depicted in Figure 45a, and their convolution results in the total spread shown in Figure 45b. To optimize computational efficiency, an analytical Gaussian approximation was employed to evaluate the total spread within the code. These corrections contribute to a more precise representation of the solar flux distribution in the model.

Figure 45: Incident radiation angular spread: components (top), and total convolved spread and Gaussian fit (bottom)

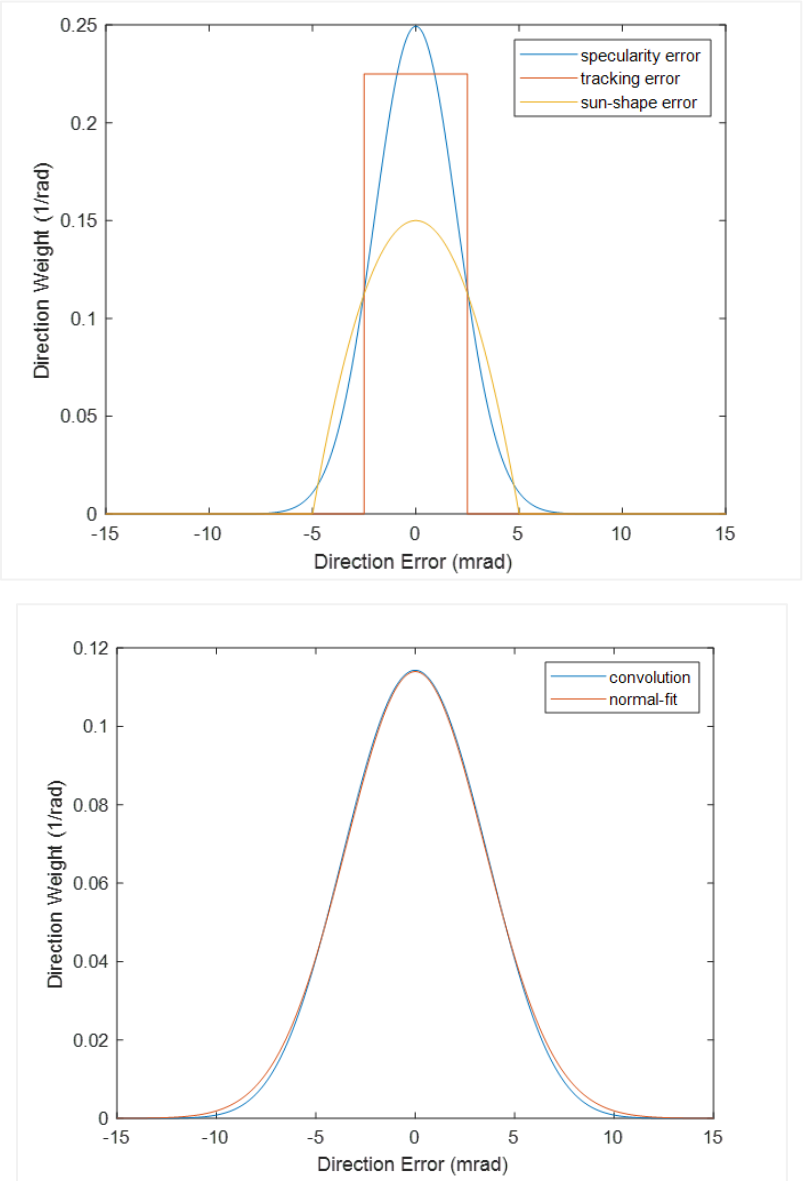

Modeled performance and absorber length optimization

The collector was modeled using the parameters presented in Table 1.

Table 1: Parameters used in the results

Parameter	Description	Value	Unit
r_o	Outer radius of absorber	21e-3	m
r_i	Inner radius of absorber	18.5e-3	m
k_{th}	Thermal conductivity of absorber	16.2	W/m-K
h_f	Heat transfer coefficient of fluid	539.435	W/m2-K

Parameter	Description	Value	Unit
c_p	Specific heat capacity of the fluid	880	J/kg-K
$\dot{m}$	Mass flow rate of the fluid solution	0.2771953	kg/s
T_f^{inlet}	Fluid inlet temperature	923.15	K
$T_{ambient}$	Ambient temperature	308	K
ϵ	Emissivity	0.1839	-
L	Length (5 different values were used in the analysis)	2, 2.5, 3, 3.5, 4	m

Figure 46 presents the modeled optical efficiency for the collector, including the effects of deformation caused by gravity and thermal expansion. The analysis considers five different absorber lengths, and it is observed that shorter absorber lengths result in reduced deformation and higher efficiency. However, there is a trade-off in terms of active absorber area, as shorter lengths lead to a decrease in the fraction of active length due to coupling between absorber segments. The combined efficiency is obtained by multiplying the intrinsic optical efficiency with the fraction of active length, and an optimum segment length between 2.5 to 3 meters was determined.

In addition to the optical considerations, practical constraints also influence the choice of absorber length. The absorber assembly needs to be mounted to the primary reflector, specifically at the gusset plates located at the intersection of the space frame and primary reflector segment joints. Considering that the primary reflector segments have a spacing of 1.45 m, choosing a multiple of this length allows for convenient integration of the absorber with the primary reflector. Thus, a length of 2.7 m for the absorber, along with 0.2 m for the coupler, is selected to optimize optical efficiency while ensuring ease of mounting.

Figure 46: Optical efficiency variance with respect to length

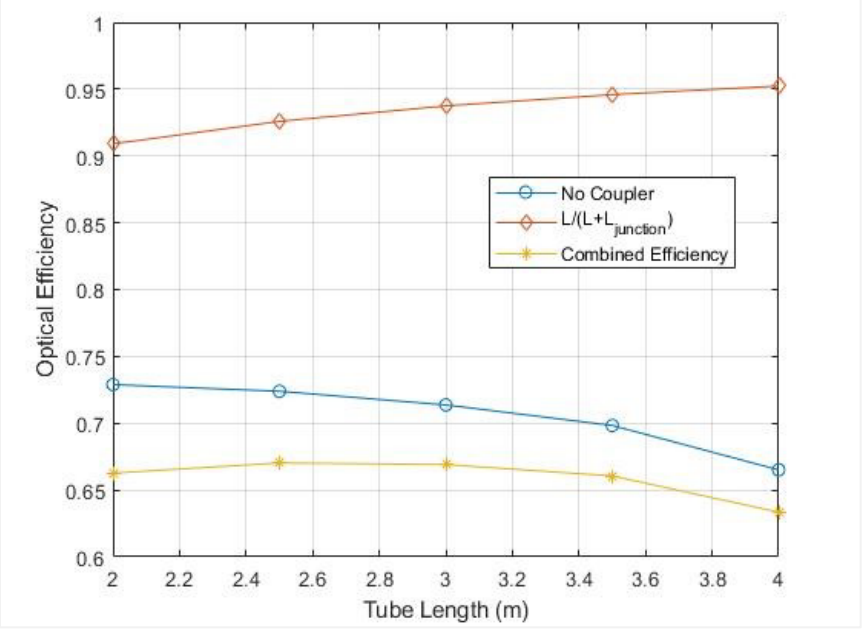

CHAPTER 4:
Particle Thermal Transfer System

Figure 47 presents a simplified flow diagram illustrating the overall particle TTS system. It is worth noting that additional valves can be incorporated to facilitate the direct transportation of particles from the storage hopper to the particles to process HX, as required. Detailed specifications for the system were developed, encompassing parameters such as air and particle flow rates, system heat balance, hopper, and piping sizes, etc. Furthermore, a control scheme for managing day-night transitions and seamless integration with the kettle controls was defined.

Figure 47: Simplified process flow diagram of the particle TTS system

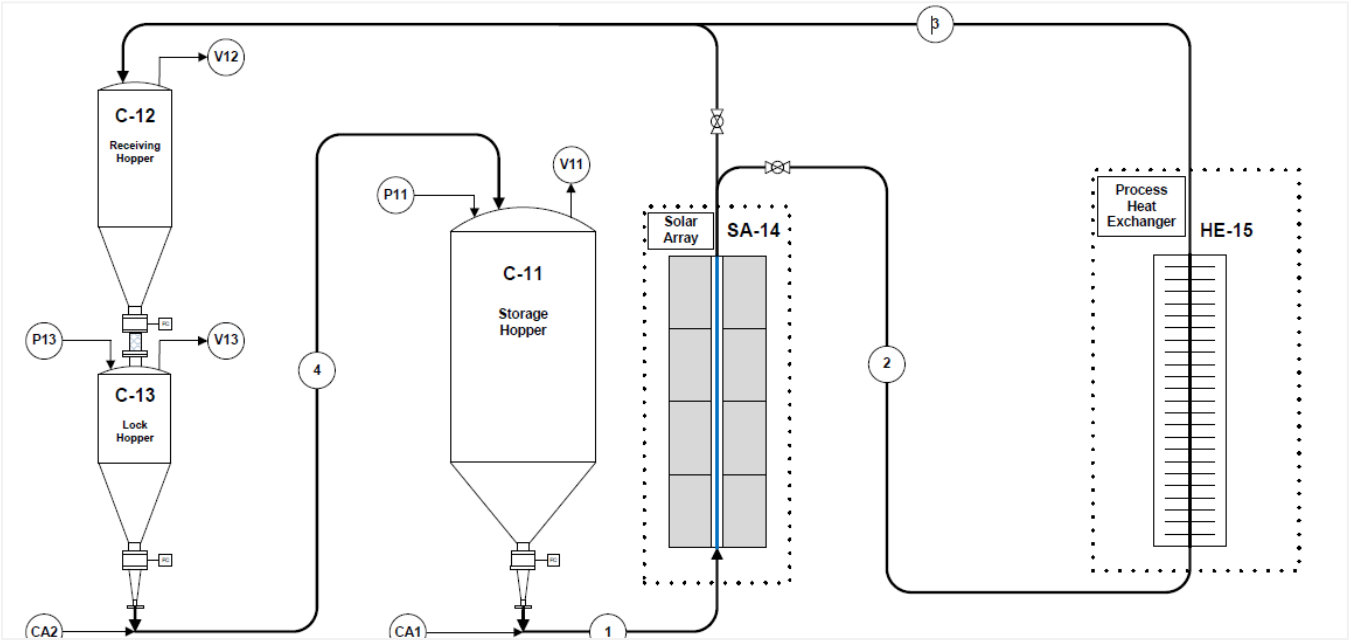

Source: GTI

Particle TTS System design, fabrication, and testing

The particle TTS system comprises storage, receiving, and lock hoppers, along with piping and controls, designed to capture energy from various sources and use inert refractory particles to store and recover the thermal energy.

For the installation of the particle TTS loop, an appropriate outdoor location was identified at GTI. This location facilitated a longer pipe run between the storage and the receiving hoppers, simulating the planned piping layout for the USG site to a reasonable extent. The piping layout at USG, shown in Figure 48 was specifically designed to achieve dense phase flow of particles through the absorber and the process HX to maximize heat transfer rates during both heat capture in the absorber and heat release in the kettle. Particulate Solids Research, Inc. conducted detailed calculations of particle suspension flow rates and pressure drops using their existing proprietary model to assist with the design of the USG piping layout. Figure 49 pre-

sents the results of pressure-velocity calculations for this layout to facilitate optimal system performance.

Figure 48: Proposed USG piping layout

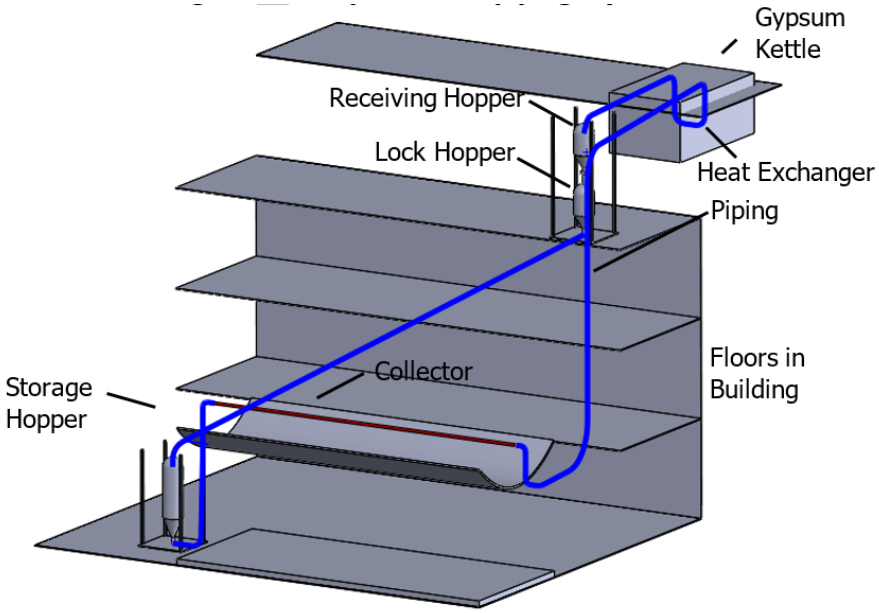

Figure 49: Pressure and velocity along the piping from the storage to the receiving hopper

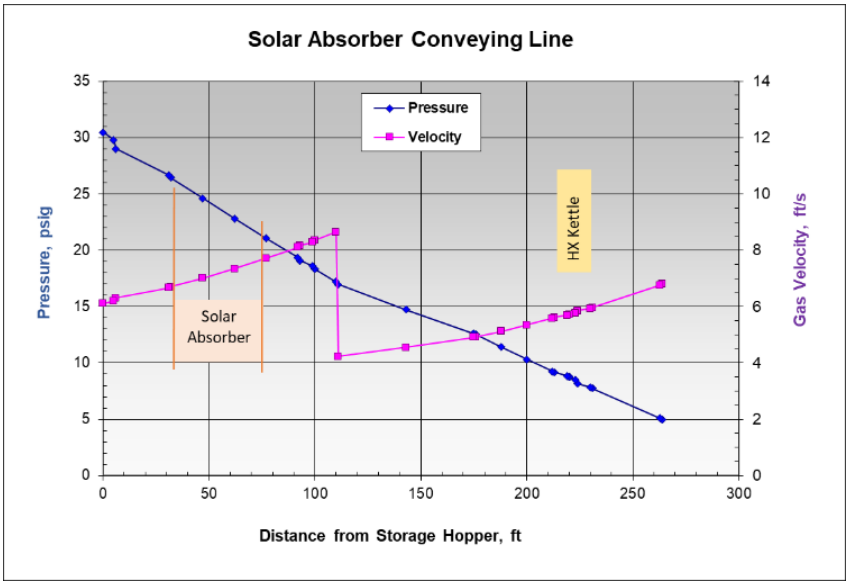

To ensure stable flow of the particles and avoid any transition from dense phase to dilute phase, which could cause flow perturbations, the diameter of the transport pipe was increased after a certain distance from the storage hopper exit. This was done to accommodate the expansion of carrier air as its pressure decreases along the flow path. This design adjustment maintains the suspension velocity in the dense phase regime, preventing uneven particle flow rates that could occur during a phase transition.

The storage, receiving, and lock hoppers for the particle TTS system were designed, fabricated, installed on skids, and insulated. To simplify the testing process and reduce costs, it was decided not to heat the particles during these tests. Since the system is sized for a nominal 50 kWth collector, heating the particles to 1,202 °F (650 °C) would require a large heating system, which would complicate the design, increase efforts, and incur additional costs. Moreover, the ability to heat and effectively transport the particles had already been demonstrated in the previous phase of the ARPA-E funded project.

Figure 50 provides an overview of the relative placement of the particle TTS system hoppers at GTI, with one skid containing the storage hopper and the second skid housing the stacked receiving (top) and lock (bottom) hoppers, along with the supply and return piping and controls. As planned for the USG setup, the pipe diameter was increased approximately halfway between the storage and receiving hoppers to maintain the desired particle-air suspension velocity in the dense phase regime. Figure 51 shows a different perspective of the particle TTS loop during the flow characterization testing, displaying power supply cables and compressed air supply hoses on the right. These tests were initially conducted in manual mode to determine the appropriate pressure, air flow rates, and pressurization timings for achieving a stable particle flow rate. Once these parameters were established, the system was programmed and operated in automatic mode.

Figure 50: Piping layout between the storage hopper skid (left) and stacked receiving and lock hopper skid (right)

Source: GTI

Figure 51: Particle TTS loop during testing

Source: GTI

Table 2: Particle flow characterization test results with manual operation provides a summary of the test results obtained during manual operation of the particle TTS system. While the designed air flow rate for effective dense phase particle transport was approximately 25 kilograms per hour (kg/hr), the initial particle flow characterization tests were conducted at lower air flow rates. These lower rates led to higher particle to air loading ratios, which are beneficial in terms of higher heat transfer rates and reduced carrier air requirements and the associated pumping power. The lower flow rates though resulted in unstable particle flow,

leading to stalling and even line plugging. The last four tests, which were conducted at close to the design air flow rate, demonstrated stable particle flow rates. The particle loading ratios during these tests ranged from 74 to 112, aligning with the specifications of the USG loop design. Additionally, the hopper pressure during these tests fell within the range of 13 pounds per square inch, gauge (psig) to 16 psig, which also is consistent with the USG loop design specifications.

Table 2: Particle flow characterization test results with manual operation

Feed air flow rate (kg/hr)	Storage hopper pressure (psig)	Particle flow rate (kg/min)	Particle to air loading ratio	Flow quality
14	23	109	469	Intermittent stalling
11	14			Plugged
11	18	48	263	Intermittent stalling
10	17	39	233	Intermittent stalling
26	16	38	89	Stable
25*	16	47	112	Stable
27	14	33	74	Stable
27	13	34	77	Stable

*Design flow rate

Figure 52 shows the particle flow rate as a function of storage hopper pressure. As expected, increasing the hopper pressure increases the particle flow rate.

Figure 52: Particle flow rate increases with increasing hopper pressure

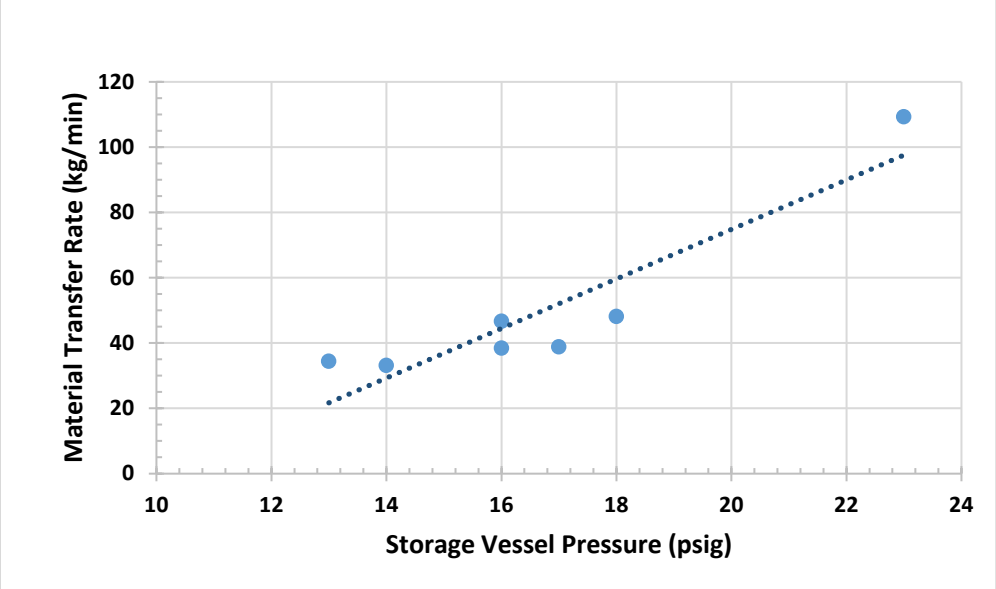

Following the characterization of particle flow performance, the particle TTS loop underwent continuous automated operation testing, consisting of 77 charge-discharge cycles conducted in four test series. The results of these tests are presented in Table 3: Particle flow characteriza-

tion test results with automated operation. Throughout these tests, the flow quality remained stable, and no problematic particle accumulations were observed, despite some adjustments made during operation to the feed air flow rate and storage hopper pressure. On average (see Table 3), the feed air flow rate was measured at 26.7 kg/hr, while the particle flow rate was 30.95 kg/minute (= 1,857 kg/hr), resulting in a particle to air mass loading ratio of 69.5 [1857/26.7].

Table 3: Particle flow characterization test results with automated operation

Test series (number of cycles)	Feed air flow rate (kg/hr)	Storage hopper pressure (psig)	Particle flow rate (kg/min)	Particle to air loading ratio	Flow quality
1, 15 cycles	24.5	13.1	27.5	67.3	Stable
2, 12 cycles	27.4	13.3	31.3	68.5	Stable
3, 25 cycles	26.9	12.8	31.0	69.1	Stable
4, 25 cycles	27.9	14.1	34.0	73.1	Stable
Average	26.7	13.3	30.1	69.5	

Upon completion of the tests, the before and after particle samples were sent to an independent laboratory for particle size characterization. Using a laser diffractor instrument, the samples were analyzed to determine the volume distribution of particles based on the laser diffraction pattern of particles suspended in a liquid. Magnified pictures of the pre- and post-test particle samples are shown in Figure 53. While there was a slightly higher volume of smaller particles in the post-test sample, which can be attributed to attrition, the overall impact on the size distribution was minimal. Importantly, there was no evidence of foreign matter presence, such as particles resulting from attrition of piping, fittings, or valves.

Figure 53: Four times micrographs of pre-(left) and post-test particle samples

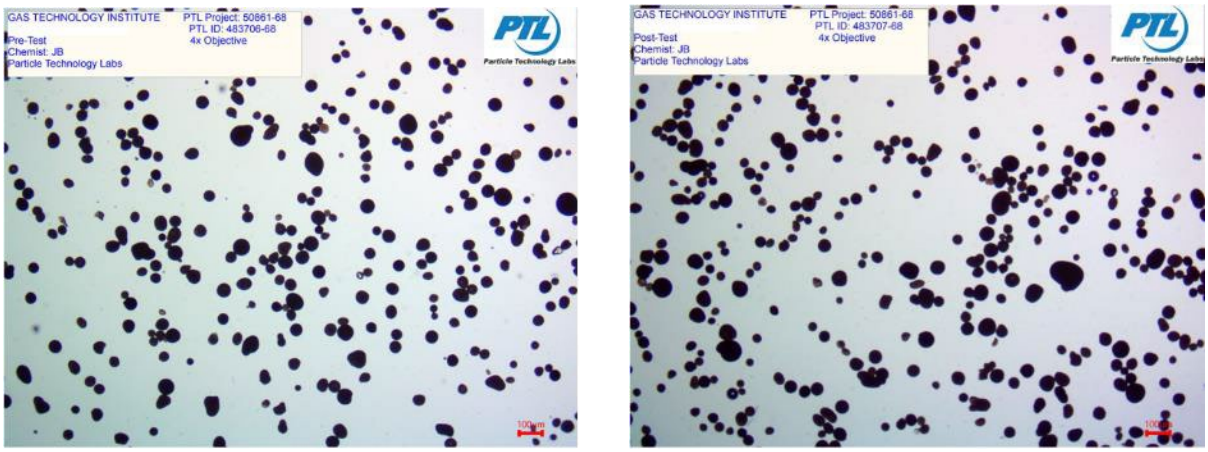

Source: GTI

Table 4: Particle size distribution of pre-and post-test samples provides a detailed analysis of the size distribution results, indicating the percentage volume of particles below various micron sizes. Notably, both the pre-test and post-test samples had no particles below 27.4 microns

(µm). In the pre-test sample, 100 percent of the particles were below 211 µm, while in the post-test sample, 100 percent of the particles were below 186 µm. Although there was a slight reduction in particle size after the tests, the overall impact was minimal.

Table 4: Particle size distribution of pre-and post-test samples

Size (µm)	Pre-test, % volume under	Post-test, % volume under
27.4	0.0	0.0
31.1	0.31	0.36
35.3	1.65	1.82
40.1	4.86	5.26
45.6	10.67	11.42
51.8	19.38	20.57
58.9	30.70	32.38
66.9	43.81	45.89
76.0	57.47	59.77
86.4	70.34	72.61
98.1	81.28	83.27
111.0	89.60	91.11
127.0	95.13	96.11
144.0	98.23	98.74
163.0	99.59	99.77
186.0	99.97	100.0
211.0	100.0	100.0

Figure 54 is a plot of particle size distribution data in Table 4, which further illustrates the small overall difference in pre-and post-test particle size distribution.

Figure 54: Pre-and post-test particle size distribution

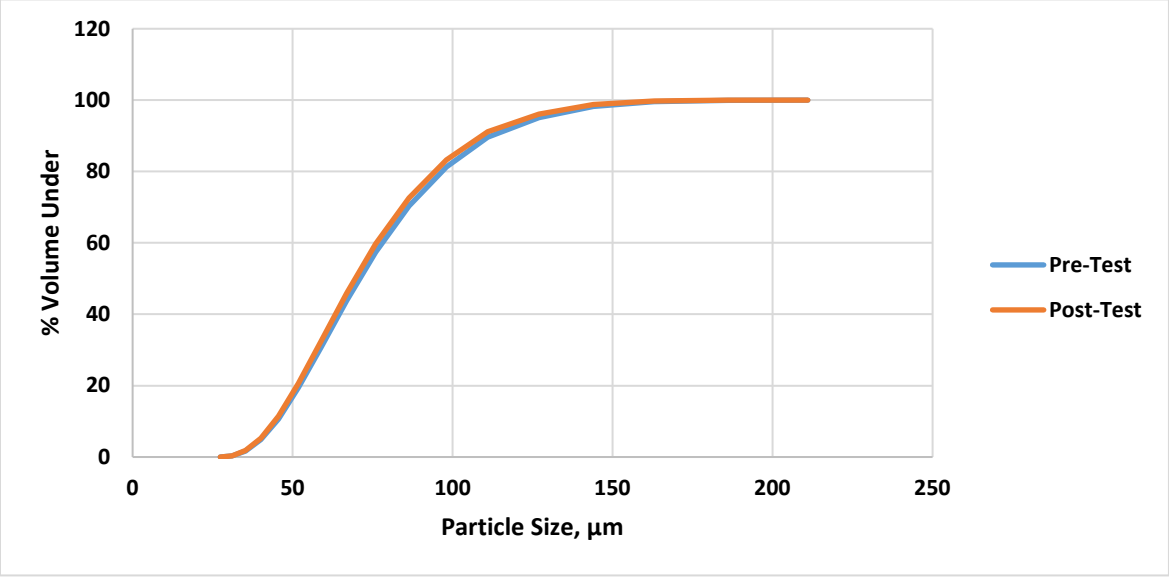

Table 5 provides a summary of the particle size distribution results, indicating the size at which 10%, 50%, and 90% of the particles in the sample are smaller than. In the pre-test sample, 90% of the particles by volume were smaller than 113 µm, 50% smaller than 70.9 µm, and 10% smaller than 44.9 µm. The last two columns present the mean particle diameters of the samples on a surface area and volume weighted basis. The difference between the pre-test

and post-test samples was approximately 2%, indicating a minimal change in the overall particle size.

Table 5: Summary of pre- and post-test particle size distribution results

Sample	Cumulative volume, 10 % below	Cumulative volume, 50 % below	Cumulative volume, 90 % below	Surface weighted mean diameter	Volume weighted mean diameter
Pre-test, µm	44.9	70.9	113	75.4	66.9
Post-test, µm	44.3	69.9	109	73.8	65.7
Difference, %	1.3	1.4	3.5	2.1	1.8

Table 6 presents a comparison between the results of the particle TTS loop tests conducted in continuous automated mode and the planned milestone targets. The particle TTS loop successfully achieved the planned test targets. The particle degradation was determined by calculating the percentage reduction in mean particle diameter in the post-test sample compared to the pre-test sample. The pumping power was calculated as the power required to pressurize and supply the carrier air for particle supply and return, assuming continuous operation of the particle TTS loop for 24 hours a day. It should be noted that if the particle TTS loop operates for fewer hours, such as during solar collection only, the pumping power will decrease proportionally.

Table 6: Comparison of particle TTS Loop testing results with test targets

Milestone parameter	Target	Results
Number of charge-discharge cycles	50	77
Particle degradation*	<5%	~2%
Pumping power as percent of thermal power	<5%	3.5%
Particle accumulation**	No problematic	No problematic

*Reduction in mean particle diameter, **Degradation of flow stability

After the successful completion of testing, preparations were made to transport the particle TTS Loop to UCM for integrated system testing. As part of this process, reinforcements were designed, fabricated, and installed to facilitate lifting and loading of the hopper skids, ensuring their protection during transportation. Specifically, shipping supports were designed and fabricated for the storage hopper skid. Lifting lugs were welded onto the storage hopper to facilitate the handling process. These measures were taken to ensure the safe and secure transport of the particle TTS Loop.

CHAPTER 5:
Conceptual Engineering of 50 kWth and 2 MWth Systems

The conceptual engineering effort was based on the system designs discussed earlier for the USG reference site. The core concept involves collecting solar energy using parabolic mirrors and secondary concentrators to heat a particle thermal fluid and transferring it to a process heat exchanger installed in USG's primary gypsum kettle. This solar energy would offset the need for natural gas in heating the USG's gypsum kettle. The system design employs pneumatic dense phase transport of alumina-based refractory particles, which are heated from 932 °F (500 °C) to 1,166 °F (630 °C). Stainless steel is used for the transport pipe and storage vessels to accommodate the elevated temperatures involved.

Conceptual engineering focused on two reference plants: Reference Plant A with a single 17.7 meter-long solar receiver, and Reference Plant B with ninety 17.7-meter-long solar receivers and six hours of thermal storage. For each plant, a process flow diagram with material/energy balance, project definition outlining project requirements, initial design basis, system sizing, construction materials, code requirements, layout, and operation were developed. Additionally, a conceptual schedule and cost estimate were provided for each plant as part of this engineering phase.

Process flow diagram and energy balance

The goal of the conceptual engineering phase was to transfer at least 40 percent of the energy collected by the solar collector(s) to the process. For the 50 kWth system, the calculated values indicate a solar to thermal efficiency of 70 percent. The heat transferred to the process during daylight hours is 50.52 kWth, and no thermal storage is used in this configuration.

For the 2 MWth system, the calculated solar to thermal efficiency was 69 percent. The heat transferred to the process is 2,020 kWth, assuming nine hours of daylight and six hours of thermal storage. In this case, a thermal storage system was implemented for six hours. The representative process considered is USG's gypsum kettle at the reference site, which is normally heated by a 30 MMBtu/hr (8.7 MWth) burner. The burner firing is reduced when the solar system is in operation, and the process temperature is maintained at 356 °F (180 °C).

Schedule

The schedules for the 50 kWth and 2 MWth plants are structured under the assumption that the installation contractor will procure all the equipment except the solar collectors, which would be purchased separately due to their potential long lead time. If the procurement of solar collectors is included in the installation contractor's scope, the schedule would extend by six to nine months.

For the 50 kWth system, the estimated total duration from the beginning of final preliminary engineering to operation is 17 months.

For the 2 MWth system, the estimated total duration from the beginning of final preliminary engineering to operation is 24 months.

Cost estimate

Cost estimates were developed using a front-end loading-1 (FEL-1) approach for both the 50 kWth and 2 MWth systems (Table 7), considering their respective requirements and configurations. In the case of the 50 kWth plant, being located adjacent to the process building resulted in a shorter piping length of 265 ft, using small-bore stainless steel piping. On the other hand, the 2 MWth plant, which is situated farther away at the USG reference site, required 1,660 ft of 12-inch stainless steel piping to connect the solar field to the process. Additionally, the solar field necessitated 8,543 ft of small-bore stainless steel piping and 4,717 ft of large-bore stainless steel piping to link the collectors to the headers.

Table 7: Summary of FEL-1 system costs

System	Cost, $
50 kWth	340,000
2 MWth with storage:	18,750,000
2 MWth without storage:	14,560,000

It is worth noting that the cost of the 2 MWth system exceeded expected values primarily because of the inclusion of thermal storage, which amounted to $4,190,000. This thermal storage enabled the system to operate for up to six hours after the solar field ceased collecting solar energy. However, removing the thermal storage would increase the energy supplied to the process during daylight hours to 3.33 MWth (with the average remaining at 2 MWth). This configuration would be suitable for process heating applications such as USG's gypsum kettle, where the solar collectors contribute a small fraction of the overall process heating requirements.

CHAPTER 6:
Preliminary Engineering of a 2 MWth System

The preliminary engineering effort built upon the conceptual engineering work for the 2 MWth system without thermal storage. This package includes the following parts:

- Updated and refined project definition
- Updated project schedule
- Updated project cost estimate
- Piping and instrument diagrams
- Equipment List with data sheets for major equipment.
- Electrical single-line diagram
- Equipment layout/general arrangement

Process flow diagram and energy balance

The system design achieved a total piping pressure drop of less than 80 psig for the transportation of heat transfer particles. This allowed for the elimination of the hot side storage vessel and air compressors. The removal of the hot side storage vessel and air compressors saved on capital costs and reduced heat losses in vented hot air and surface radiation from these vessels and associated piping. These heat loss savings contribute to an overall increase in system efficiency.

- For the 2 MWth system without thermal storage, the calculated values are as follows:
- Thermal efficiency: 73 percent
- Heat transferred to the process: 2,979 kWth (assuming nine hours of daylight)
- Thermal Storage: None

Like the 50 kWth system, the representative process for the 2 MWth system is assumed to be USG's gypsum kettle at the reference site.

Schedule

As with conceptual engineering, the schedule for the 2 MWth plant assumes that the installation contractor will procure all the equipment except for the solar collectors. Since solar collectors often have a longer lead time, they would be purchased separately. However, if the procurement of solar collectors is included in the contractor's scope, the schedule would be extended by six to nine months to account for the additional time needed.

The total duration for the 2 MWth system, starting from the beginning of final preliminary engineering to the operation phase, is estimated to be 24 months.

Cost estimate

Cost estimates were developed for systems, both with and without thermal storage, and adjustments were made to the solar field and piping configurations during the front-end loading-2 (FEL-2) phase. The solar field was relocated to the north of the gypsum storage shelter to prevent shading and improve space utilization, which required additional receiver feed piping and header piping. The total estimated header piping between the solar field and the process heat exchanger is 2,762 ft of 10-inch and 12-inch diameter. The configuration of the piping in the solar field was also modified to balance the flows. The solar field requires approximately 3,140 ft of small-bore stainless steel piping and 5,906 ft of large-bore stainless steel piping to connect the solar collectors to the headers.

The elimination of the hot side storage vessel and associated air compressors resulted in cost savings in the estimate. However, the overall cost estimate increased due to the significant increase in piping costs caused by longer pipe lengths and higher stainless steel prices. The preliminary engineering cost estimate for the 2 MWth system without storage is $17,620,000, representing an increase of $3,060,000 compared to the conceptual engineering cost estimate.

The techno economic analysis (TEA) Model, which uses the system advisor model developed by the National Renewable Energy Laboratory, provided a lower cost estimate of $3,808,603 for the 8.7-acre solar field (without thermal storage cost). However, the system advisor model was based on 2015 dollars and used outdated pricing information from a company that may no longer be in business. Considering annual escalation and the current Chemical Engineering Plant Cost Index, the TEA model estimate would increase to around $5,332,000.

One significant factor contributing to the differences between the preliminary engineering and TEA cost estimates is the substantial increase in stainless steel prices since 2015. Stainless steel is extensively used in this project for piping and vessels due to the elevated temperatures involved. The price of stainless steel has experienced a significant rise, reaching $1.82 per pound in June 2022, a 240 percent to 479 percent increase compared to the prices in 2015. This price increase could account for the notable difference between the TEA model and preliminary engineering cost estimate. It should be noted that stainless steel prices have started to decrease from their peak in July and August 2022, which could potentially lead to a reduction in project costs.

A detailed comparison of the differences between the preliminary engineering cost estimate and an earlier TEA model estimate is presented in Table 8.

Table 8: High temperature solar receiver cost estimate comparison to TEA

	Cost Estimate - Without Storage	TEA 1/31/22	Notes
Civil	325,904	281,873	
Solar Field	3,336,024	1,343,968	Major cost difference is in foundations. Cost estimate has 50% of cost as foundations ($20,350/mirror). TEA has $902/mirror. Foundation is based upon drilled pier. Another option is to drive

	Cost Estimate - Without Storage	TEA 1/31/22	Notes
			pipe piles. Driven pipe piles required adding welded baseplate to even up and match bolt holes of mirror structure.
Receiving Hoppers	414,464	164,584	Need additional support steel to elevate. Stainless steel price increase.
Cyclone Separator	38,073	409	$409 seems very low
Air Compressors	104,831	46,911	
Heat Exchanger	118,050	3,051	$3,051 seems very low
Transport Piping	2,415,228	615,238	Stainless steel piping Increase
Solar Array Piping	2,064,838	198,438	Piping size/length required increase substantially going from one mirror to 90 mirrors.
Instrument & Controls	196,700	58,483	More instruments needed to verify balanced flow between mirrors and to control the vessel/lock hopper system.
Electrical	211,332		TEA does not appear to include electrical cost
Particles	21,876	41,432	
SUBTOTAL	**9,247,320**	**2,754,388**	
Escalation of 3.5% from 2015 to 2021		3,385,846	
Escalation of 20% in 2022		4,063,015	
Escalation of 10% is 2023		4,469,316	
Mobilization - 3%	277,420		
Sales Tax, 5%	290,637	211,896	
Supply Chain Interruption - 10%	952,474		Covering potential price increases.
Contingency - 10%	1,047,721	446,932	Used same percentage
Contractor Overhead - 15%	1,728,740		Cost estimate has separate markup for contractor overhead
Contractor Profit - 10%	1,325,368		Cost estimate has separate markup for contractor profit
TOTAL DIRECT CAPITAL COST	**14,869,680**	**5,128,144**	
Engineering (1.5% of solar collector, 6% on BOP)	604,452	98,325	TEA has 2%, Cost Estimate has 1.5% on solar collector and 6% on BOP
on TEA.			
Owners Engineering & Project Management, 7%	1,040,878	344,137	Both use same percentage of 7%
Construction Management 1.6%	237,915	78,660	Both use same percentage of 1.6%

	Cost Estimate - Without Storage	TEA 1/31/22	Notes
Commissioning/Startup 0.2%	29,739	9,832	Both use same percentage of 0.2%
Interest During Construction, 4%	594,787	196,650	Both use same percentage of 4%
Permitting, Licensing, Legal 1%	148,697	49,162	Both use same percentage of 1%
Land purchasing	90,000	88,167	Cost estimate rounded up to $10,000/acre
TOTAL INDIRECT CAPITAL COST	**2,746,468**	**864,934**	
PROBABLE CONSTRUCTION COST	**17,620,000**	**5,993,079**	

BOP = balance of plant

CHAPTER 7: Technology/Knowledge/Market Transfer Activities

In this task, the team focused on developing an updated STTS technology commercialization plan, customer engagement plan, and cost analysis, while also evaluating market trade-offs and manufacturing considerations.

Commercialization plan

GTI collaborated with the University of Chicago Booth School of Business and Stanley to conduct a comprehensive assessment aimed at determining the optimal strategy for commercializing the STTS technology. The project encompassed various key aspects, including: defining the product and services to be offered, identifying market drivers for the technology, formulating an operations plan, outlining a research and development roadmap, devising a distribution strategy, assembling an operations team, conducting a market analysis, developing a marketing approach, evaluating competition and the competitive landscape, constructing a financial model, performing a valuation, exploring licensing options, preparing a venture capital pitch, and conducting an exit analysis.

To gather valuable insights and feedback, twelve industry leaders from diverse market sectors were interviewed. The findings from these interviews were used to explore paths forward. Two primary options considered were entering into licensing arrangements or establishing a GTI subsidiary dedicated to the commercialization of the technology. These options will be carefully evaluated based on the insights gathered and the results of any future on-sun integrated system testing and process heating field demonstration to select the commercialization path.

Product and services

The product offering consists of a 2 MWth high-temperature solar-energy driven supplemental process heating system with the option for up to six hours of thermal storage. This system will be designed to provide efficient and reliable heating solutions for clients. The product package will include the necessary system equipment, infrastructure, and land required for installation. Additionally, GTI will provide supervision and assistance during the installation and startup phases to ensure a smooth and successful implementation.

Market drivers

The market drivers for the high temperature STTS technology stem from the technical and environmental challenges faced by the current state of the art industrial heating systems.

Technically, existing systems encounter issues such as corrosion, system stress, limited temperature and pressure ranges, low efficiency, and limits on plant's natural gas use. These limitations hinder the effectiveness and reliability of the current technologies and prevent production increases.

Additionally, the environmental impact of traditional heating systems, including greenhouse gas emissions, drives the demand for greener energy sources. The high temperature STTS should integrate well into industrial processes, providing supplemental thermal energy and process heating using a non-corrosive, low-cost, low-pressure, and non-flammable particle thermal fluid. With advantages like increased solar concentration, inert and stable fluids, dispatchable and modular capabilities, and reliance on renewable energy sources, the high temperature STTS will offer a compelling solution that addresses the market's need for improved efficiency and reduced environmental impact.

Operations plan

The operations plan for the high temperature STTS technology involves several crucial steps to ensure its successful implementation and ongoing support. This includes identifying manufacturers for proprietary equipment and auxiliary components, bidding and executing contracts for equipment production, and developing service contracts with customers. The construction and assembly phase will involve procuring and preparing the land, supervising onsite installation, and hiring local support staff as needed. Ongoing operations and maintenance support will be provided, including performance monitoring, process improvement assistance, and systematizing heat transfer fluid orders.

By following this operations plan, the high temperature STTS technology can be efficiently deployed and maintained. It will ensure effective coordination with manufacturers and contractors, customization of systems for clients' needs, and the provision of continuous support throughout the system's lifespan. This approach will facilitate smooth operations, maximize system performance, and provide customers with reliable, sustainable, and cost-effective thermal energy solutions.

Research and development roadmap

A four-year roadmap was developed outlining key objectives for optimization, continuous improvement, and technology expertise to guide the commercialization of the high temperature HSS technology. This roadmap encompasses strategic planning to address human and financial resource requirements, as well as technological advancements necessary for the successful progression of the technology towards widespread adoption in the market. GTI is currently advancing the particle TTS technology for industrial heat recovery in a follow-on project funded by the US Department of Defense through Worcester Polytechnic Institute.

Distribution strategy, operations team, market analysis

The initial target market for the high temperature STTS technology will be food manufacturing sites located in sunny geographies. The global food market, with a compound annual growth rate of 4 percent, reached approximately $4 billion in 2020. The food industry alone accounts for a significant amount of process heating and offers various process types that are well-suited for supplemental process heating, including sterilization, pasteurization, ultra-high temperature processing, and pet food rendering. To capture this market, marketing and sales efforts will focus on identifying and engaging potential clients in the food industry, leveraging the results from pilot plants to effectively demonstrate the benefits and efficacy of the

product. Geographically, regions with ample sunlight and a strong presence of food manufacturing and processing include California, Colorado, Arizona, and Utah.

In addition to the food industry, other heat-intensive processes such as gas-fueled process heating furnaces, steel and metals manufacturing, thermal storage, and commercial heating, ventilation, and air conditioning systems present potential market opportunities for the high temperature STTS technology. These industries will be considered for future expansion and diversification of the technology's applications. Industrial process heat recovery is another potential market for the particle TTS system.

Marketing approach and trade-offs

The marketing approach for the high temperature STTS technology encompasses customer acquisition, retention, and growth strategies, with a particular focus on pilot programs. The decision-making unit consists of multiple stakeholders, including the buyer (manufacturing and procurement managers), user (engineering and capital projects groups), and influencer (controllers and marketing managers). The decision-making process aligns with the company's capital projects process that typically spans around six months and involves close collaboration between the customers and the company's capital projects team.

Although customer acquisition costs may be relatively high, the costs are justified by the high customer lifetime value resulting from projected customer retention rates and annual profits. This tradeoff acknowledges the initial investment required to acquire customers but recognizes the long-term value that can be gained through ongoing relationships and consistent revenue generation. By prioritizing customer acquisition, retention, and growth, the marketing approach aims to establish strong partnerships with customers, maximize their satisfaction, and ensure sustainable profitability for the business.

Competition and competitive landscape

In the competitive landscape, the primary competitor for supplemental heat applications is natural gas, which is widely used in various industries. However, the high temperature STTS technology also faces competition from other sources, including molten salt thermal energy storage, other refractory material storage technologies, process heat integration solutions, and concentrated solar power plants. These alternatives offer different approaches to addressing heat requirements in industrial processes and provide alternative options for customers seeking heat generation and storage solutions. It is important for the high temperature STTS technology to differentiate itself by highlighting its unique features, such as its non-corrosive and low-cost thermal fluid, high efficiency, dispatchability, ability to harness renewable energy sources, and modularity of solar arrays to effectively compete in the market.

Financial model

The financial model for the high temperature STTS technology offers a stable and recurring cash flow, presenting an opportunity for partnerships and long-term financial sustainability. In terms of capital structure, there is potential to reduce the initial cash requirement through debt or equity partnerships once the technology is proven commercially viable. The partnering structure follows a well-established business model commonly employed in the renewables

sector, allowing for capital recycling and mitigating risks associated with individual projects. Despite the potential benefits, it is important to consider potential risks, such as the need for a larger balance sheet compared to pure manufacturing organizations. Additionally, reaching cash breakeven as a company requires significant scale due to the highly contracted nature of the assets.

Exit analysis

The exit analysis examined three potential exit options: strategic buyers, financial buyers, and an initial public offering. Strategic buyers, such as established manufacturers or developers with existing sales channels, offer the potential for using the technology effectively and leveraging their market presence. Financial buyers may view the technology as an attractive platform acquisition for future heating and cooling roll-ups. However, an initial public offering is deemed less favorable as an exit opportunity due to the extended timeline, limited liquidity, and the need for substantial growth and a defensible market position.

Schedule

The schedule for the 2 MWth plant is structured with the installation contractor responsible for procuring all equipment except the solar collectors. This approach allows for efficient progress as the solar collectors, which typically have longer lead times, can be purchased separately. If the procurement of solar collectors is included in the contractor's scope, the schedule would be extended by approximately six to nine months.

The estimated total duration, from the start of final preliminary engineering to the operational phase, is anticipated to be 24 months. This timeline considers the various stages involved in the project, including equipment procurement, installation, and commissioning, ensuring a comprehensive and efficient implementation process.

Manufacturing

The particle TTS system does not require specialized engineering or manufacturing processes. Its components can be readily procured off-the-shelf or fabricated without the need for special tooling. To ensure quality and competitive pricing, it is advisable to obtain multiple bids from reputable suppliers and fabricators for most of the components. The design and specifications of piping, valves, instrumentation, and vessels related to particle transport are well-established.

The parabolic trough can be sourced from an existing supplier or engineered and manufactured using standard techniques. Many companies already produce parabolic troughs, making them potential procurement sources for this component.

The receiver poses certain manufacturing challenges. While it can be fabricated using standard materials and supplies, specialized fabrication and assembly skills are required. The following components within the receiver would necessitate special tooling:

1. Glass tube: The required tube size is not standard and may not be readily available from solar glass tube manufacturers.

2. Low emissivity absorber: Due to its anticipated high operating temperature, the absorber requires a specialized low emissivity coating to minimize radiation loss. Coating the tubes requires specific equipment and expertise. Companies that use coated tubes for radiant space heating, which operate at even higher temperatures, could potentially manufacture the required absorber tubes since they have the necessary coating equipment. Although the space heating tubes are of a larger diameter (four to eight inches) and coated with a high emissivity coating, these companies are good candidates for manufacturing the required absorber tubes.
3. Secondary reflector: This component is a shaped sheet of aluminum or stainless steel coated with a highly reflective coating on one side and a high emissivity coating on the other. Numerous sheet metal fabricators would be able to readily produce these.
4. End caps and bellows: Fabrication of these components would require special tooling but can be accomplished by stainless steel parts fabricators.

It is recommended that the manufacturing partner source most of the standard components from third-party suppliers unless they already manufacture them. However, for the specialized receiver components, it is advisable for the manufacturing partner to undertake their manufacturing and assembly themselves. This is primarily due to the precision and quality control required. Alternatively, the entire receiver assembly could be fabricated and assembled by a qualified third party. In such cases, a longer-term agreement may be necessary to control costs and ensure a consistent supply, given the specialized equipment and tooling involved.

Publications and Collaborations

Journal Articles, Papers, and Thesis

1. Abdelhamid, M., B. Widyolar, L. Jiang, R. Winston, E. Yablonovitch, G. Scranton, D. Cygan, H. Abbasi, and A. Kozlov. 2016. "Novel double-stage high-concentrated solar PV/T hybrid system using nonimaging optics with GaAs cells." Applied Energy 182(15) 68-79.
2. Widyolar, B., L. Jiang, J. Ferry, R. Winston, D. Cygan, and H. Abbasi. 2019. "Experimental performance of a two-stage (50×) parabolic trough collector tested to 650 °C using a suspended particulate heat transfer fluid." Applied Energy, 240(15), 436-445.
3. Widyolar, B., L. Jiang, J. Ferry, R. Winston, A. Kirk, M. Osowski, D. Cygan, and H. Abbasi. 2019. "Theoretical and experimental performance of a two-stage (50X) hybrid spectrum splitting solar collector tested to 600 °C." Applied Energy, 239(1), 514-525.
4. Widyolar, B., L, Jiang, J. Ferry, J., R. Winston, A. Kirk, M. Osowski, D. Cygan, and H. Abbasi. 2018. "Two-stage 50X hybrid spectrum splitting CSP/CPV collector with InGaP/GaAs solar cells." In Nonimaging Optics: Efficient Design for Illumination and Solar Concentration XV (Vol. 10758, p. 1075806). International Society for Optics and Photonics.
5. Bhusal, Y., Widyolar, B., Jiang, L., Ferry, J., Brinkley, J. and Winston, R., 2019, September. High concentration parabolic trough solar collector with novel secondary in

the vacuum receiver. In Nonimaging Optics: Efficient Design for Illumination and Solar Concentration XVI (Vol. 11120, p. 1112004). International Society for Optics and Photonics.

Team member Yogesh Bhusal achieved a significant milestone by submitting and successfully defending his PhD dissertation titled 'Towards a Carbon-Free Future of Solar Thermal with Nonimaging Concentrators.' The dissertation was primarily based on the work performed in this project.

Networks/Collaborations

The project fostered networks and collaborations through various events and presentations. In November 2019, a solar symposium organized by UCM featured a discussion on higher temperature applications for solar thermal, which included the project as a topic. The symposium saw participation from ARPA-E staff, facilitating valuable connections in the field.

The project results were also presented at the ARPA-E Energy Innovation Summit in May 2021 and May 2022, held at the Gaylord Rockies Resort and Convention Center in Denver, Colorado. This forum provided an opportunity to showcase the technology to a broader audience and engage with industry professionals and experts.

Furthermore, in February 2022, a WebEx hosted by Southern California Gas Company featured the technology, serving as an important outreach effort for the project. The seminar highlighted the innovative approach of the particle TTS technology in recovering heat from commercial and industrial processes. It emphasized the potential for energy demand management, emissions reduction, and improved productivity through the recovery and reuse of waste energy. It discussed the progress made on STTS technology, underscoring its potential role in decarbonizing the existing natural gas infrastructure and its alignment with GTI's larger efforts in process heating applications. It can be viewed at: https://www.youtube.com/watch?v=ywaXVJbG530.

The collaborations and engagements through these events and presentations have helped establish connections, raise awareness, and position the project as a significant player in the field of solar thermal applications and energy innovation.

CHAPTER 8: Conclusions/Recommendations

The research and development efforts undertaken in this project have yielded significant advancements in the field of high temperature solar thermal energy. The successful testing of particle TTS technology offers opportunities for high temperature energy capture, storage, and on-demand use from solar, as well as the exhausts of industrial processes and engines. The particle TTS system worked per the design specifications in terms of carrier air flow rate, particle flow rate, and hopper pressures and flow stability, which will allow the team to scale it with confidence. GTI is advancing this technology for industrial heat recovery in a follow-on project funded by the US Department of Defense through Worcester Polytechnic Institute. The particle TTS and STTS technologies progressed in this project can make important contributions towards meeting the technical, cost, and environmental challenges faced by the process heating industry. Testing of the innovative two-stage collector at UCM and development and implementation of the associated self-consistent model have provided valuable insights into optimizing its performance for high temperature operation. Results of on-sun testing and modeling have shown the four-meter design length of the absorber/receiver is not ideal and causes significant bending of the absorber and reduced efficiency. The model developed that integrates illumination, thermal behavior, and deformation analysis modules in a single iterative algorithm has allowed optimization of the receiver-absorber specifications for optimum thermal and mechanical performance, while minimizing its bending. By combining modeling and front-end engineering efforts, the research team has addressed the absorber bending issues and provided a solid foundation for future demonstration and commercialization of the STTS technology. This approach optimized the system's performance, refined its design, and enhanced potential for successful deployment of the STTS technology.

Based on the outcomes of this project, several recommendations can be made. First, reduce the absorber length to 2.7 m to optimize its thermal-mechanical performance. Second, demonstrate the revised absorber/receiver on-sun at UCM, or at an alternate site, before pursuing field applications. Third, focus on initially targeting food manufacturing sites in sunny geographies, such as California, given the substantial market potential and the compatibility of the STTS technology with their process heating needs. This targeted approach will help maximize customer acquisition and revenue generation. Fourth, establish strategic partnerships with manufacturers for auxiliary equipment and components, such as storage tanks and air blowers, which will ensure a reliable supply chain and streamlined manufacturing processes. This will facilitate efficient project execution and deployment of the STTS technology.

Furthermore, active engagement with potential customers in the food industry and other heat-intensive sectors, such as gas-fueled process heating furnaces and steel manufacturing, is crucial. This can be achieved through pilot programs and tailored marketing strategies that highlight the unique benefits and competitive advantages of the STTS technology.

Additionally, continued research and development efforts should be undertaken to optimize the system's short- and longer-term performances, enhance efficiency, and explore potential

applications in other industries and geographical regions. Ongoing collaboration with research institutions, industry partners, and government agencies will provide valuable insights and support for further advancements.

CHAPTER 9:
Benefits to Ratepayers

Broad deployment of the STTS technology following successful implementation of the recommendations outlined earlier has the potential for significant reductions in the demand for natural gas at a wide range of industrial sites in California with operating temperatures up to 932 °F (500 °C). This will benefit natural gas rate payers by promoting more efficient use of gas and decreasing gas consumption for process heating. Industrial facilities will experience advantages such as improved energy efficiency, environmental stewardship, sustainable energy practices, reduced natural gas costs, and increased profitability. Widespread adoption of the STTS technology offers significant environmental benefits, improved performance, and life-cycle cost savings to rate payers in California, providing them with a cost-effective path towards achieving substantial energy cost reductions.

The initial target market for the STTS technology will be food manufacturing sites. As per a CEC 2020 report, California is the largest food producing state in the U.S., generating a fifth of the country's dairy products, over a third of the country's vegetables, and three-quarters of the country's fruits and nuts (CDFA 2022). California is also the largest food processing state with over 6,000 active establishments in 2019. Food processing is also a key economic sector, but also a significant contributor to greenhouse gas emissions with approximately 3.3 million metric tons of carbon dioxide equivalent emissions per year (CARB 2020).

The food industry alone accounts for a significant amount of process heating in California and offers various process types that are well-suited for supplemental process heating, including sterilization, pasteurization, ultra-high temperature processing, and pet food rendering. To capture this market, marketing and sales efforts will focus on identifying and engaging potential clients in the food industry, leveraging the results from pilot plants to effectively demonstrate the benefits and efficacy of the product. Geographically, regions with ample sunlight and a strong presence of food manufacturing and processing include California, Colorado, Arizona, and Utah.

In addition to the food industry, other heat-intensive processes such as gas-fueled process heating furnaces, steel and metals manufacturing, thermal storage, and commercial heating, ventilation, and air conditioning systems present potential market opportunities for the high temperature STTS technology. These industries will be considered for future expansion and diversification of the technology's applications. Industrial process heat recovery is another potential market for the particle TTS system.

GTI is currently demonstrating the particle TTS technology component of the STTS technology in a follow-on project funded by the US Department of Defense through Worcester Polytechnic Institute. The particle TTS technology is suitable for heat recovery from exhaust gases of a wide-range of industrial processes, both continuous and batch types, and has the potential for significant natural gas savings and carbon reductions in California.

In summary, the STTS technology, with successful implementation and testing of recommended design improvements, has the potential to revolutionize the field of process heating by offering a renewable and sustainable alternative to conventional solutions. By implementing the above recommendations, the commercialization and widespread adoption of this technology can be possible, leading to a more environmentally friendly and efficient approach to meeting industrial heating needs.

Quantitative estimates of benefits

The potential candidate industrial process heating applications for the STTS technology in California are projected to account for approximately 200 TBtu of annual natural gas use, which represents approximately 30 percent of the natural gas consumed for industrial process heating in the state. The STTS technology has the potential to deliver annual natural gas savings of over 4 TBtu in California's industrial markets, assuming a 20 percent efficiency gain and a 10 percent market penetration. These projected energy savings amount to $40 million annually for customers in California, considering a gas price of $10/MMBtu. Additionally, the implementation of the STTS technology has the potential to reduce greenhouse gas and nitrogen oxide emissions, with estimated annual reductions exceeding 42,000 metric tons of carbon dioxide equivalent emissions per year and 35 metric tons of nitrogen oxide emissions.

GLOSSARY AND LIST OF ACRONYMS

Term	Definition
Absorber	The tubular element of a solar collector that absorbs solar energy reflected to it by the primary reflector – definition used in this report
ARPA-E	Advanced Research Project Agency – Energy of the U.S. Department of Energy (DOE)
BTU/hr	British thermal units of energy per hour
°C	degrees Celsius
CARB	California Air Resources Board
CDFA	California Department of Food and Agriculture
CEC	California Energy Commission
Collector	Combination of primary solar reflector, receiver, and associated components – definition used in this report
DOE	US Department of Energy
°F	degrees Fahrenheit
FEL-1	Front-end loading -1 is the process for conceptual development of projects
FEL-2	Front-end loading -2 is preliminary equipment design, layout, schedule, and estimate
GTI	GTI Energy
HX	Heat Exchanger – commonly used terminology
Kg/hr	kilograms per hour
kg/s	kilograms per second
kWth	kilowatts thermal
m	meter
µm	micron or micrometer
m2	square meter
MM	million
MMBtu	million British thermal units of energy
MWth	pounds per square inch, gauge megawatt thermal
psig	pounds per square inch, gauge
Primary reflector	A parabolic shaped trough with mirror surface reflects and focuses sunlight on the receiver/absorber – definition used in this report
PVD	Physical vapor deposition

Term	Definition
Receiver	Element of the solar collector that receives sunlight from the primary reflector. Includes, absorber, secondary reflector, surrounding evacuated glass tube and associated components – definition used in this report
Secondary reflector	A smaller reflector within the evacuated tube that reflects sunlight from the primary reflector to the back side of the absorber - definition used in this report
STTS	Solar thermal transport and storage – System that captures thermal energy from a solar source to heat solid particles and transports these particles for storage or energy recovery equipment - definition used in this report
TBtu	trillion British thermal units of energy
TEA	Techno economic analysis is a method for evaluating the economic performance of a technology
Particle TTS	Particle thermal transport and storage – System that captures thermal energy from any source to heat solid particles and transports these particles for storage or energy recovery equipment - project definition
UCM	University of California at Merced – definition used in this report
USG	USG Corporation

References

CARB (California Air Resources Board). 2020.

CDFA (California Department of Food and Agriculture). 2022. "California Agricultural Production Statistics." Available at: https://www.cdfa.ca.gov/statistics/